Feasibility Design of a Continuous Insulin Sensor from lessons learned using Glucose sensors, and point of care insulin sensors.

by

David L Probst

A Thesis Presented in Partial Fulfillment
of the Requirements for the Degree
Master of Engineering

Approved April 2018 by the
Graduate Supervisory Committee:

Jeffery LaBelle, Chair
Micheal Caplan
Curtiss Cook

ARIZONA STATE UNIVERSITY

May 2018

ABSTRACT

Glucose sensors have had many paradigm shifts, beginning with using urine, to point of care blood, now being approved for implant. This review covers various aspects of the sensors, ranging from the types of surface chemistry, and electron transduction. All the way to the algorithms, and filters used to alter and understand the signal being transduced. Focus is given to Dr. Hellerâ's work using redox mediators, as well as Dr. Sode in his advances for direct electron transfer. Simple process of designing sensors are described, as well as the possible errors that may come with glucose sensor use. Finally, a small window into the future trends of glucose sensors is described both from a device view point, as well as organic viewpoint. Using this history the initial point of care sensor for insulin published through LaBelle's lab is reevaluated critically. In addition, the modeling of the possibility of continuously measuring insulin is researched. To better understand the design for a continuous glucose sensor, the basic kinetic model is set up, and ran through a design of experiments to then optimized what the binding kinetics for an ideal insulin molecular recognition element would be. In addition, the phenomena of two electrochemical impedance spectroscopy peaks is analyzed, and two theories are suggests, and demonstrated to a modest level.

ACKNOWLEDGMENTS

I would like to acknowledge both Arizona state university, for allowing me to perform this work as well as the incredible opportunities and mentorship received form Labelle. In addition, there are various other people who have enabled this work; Thanks to Dr. Lin, Mackenzie Honikel, Brittney Cardinal, Michael Caplan, Curtiss Cook and the Mayo Clinic. In addition, thank you to the incredible Shelby Steed for all the support and never-ending positive attitude toward my work.

TABLE OF CONTENTS

Page

LIST OF TABLES

LIST OF FIGURES

Figure Page

CHAPTER 1

REVIEW OF GLUCOSE SENSORS

The world of biosensing has quickly been gaining momentum over the last few decades as a method for diagnosing, monitoring, and recently remotely monitoring various disease states. These sensors have utilized various fields of physics from radiation, magnetics, resonance, and electrical. Each of which had defining moments that can be traced back to where most of today's techniques can be either directly, or indirectly linked to. Most biosensor platforms have had these defining moments where the potential was unveiled. Enzyme linked immunosorbent assay (ELISA) for example, was first described in 1960 by Peter Perlmann and Eva Engvall at Stockholm University ([1]). Famously for electrochemical sensors as well as for most sensors is the point of care and continuous glucose sensor. This is due to the amount of research, and development that has been performed to these devices in both industry, as well as academics. Glucose sensors make up for probably the most researched biosensors of all time, including a phenomenal timeline for their development (Figure 1).

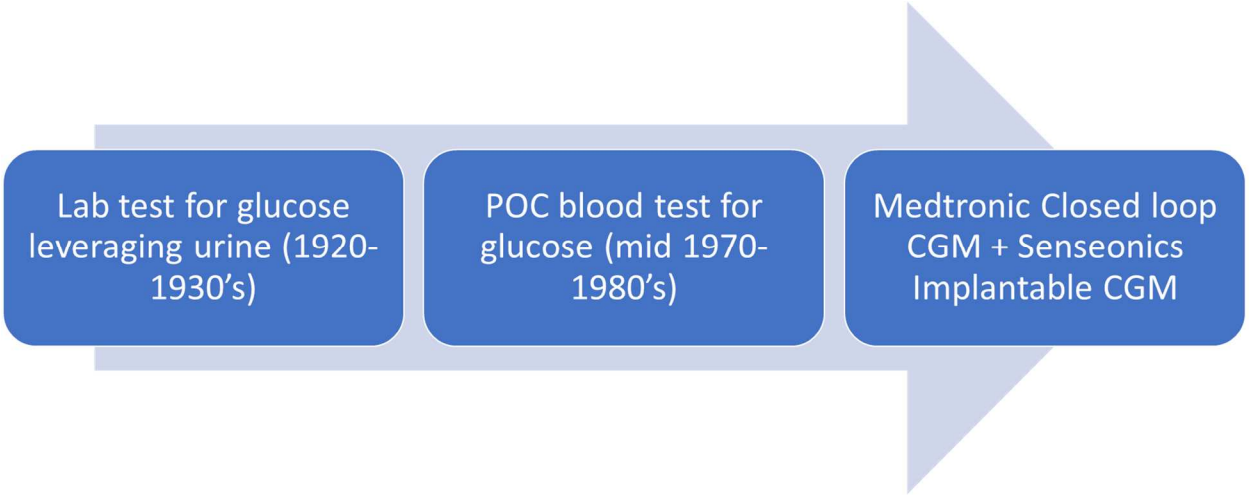

Figure 1: General timeline for the development of the current "gold standard" glucose sensor. This begins back in the early 1920's where the use of urine was employed for glucose. Then nearly 50 years later the first commercially available glucose sensors where designed employing 1st generation sensing. Finally, just recently, Medtronic released the first closed loop CGM therapy combination for type 1 diabetics as well as Senseonics receiving FDA approval for a 90 day implantable sensor [2],[3].

Glucose sensors were first proposed by Clarke and Lyon in 1962 in Cincinnati [1] as well as a description of what the "biosensor" system may look like. This discovery lead to the explosion of research on applying electrochemistry to biosensors, and analyte detection. So rapid that it was just a few years later in 1973 that the first hydrogen peroxide glucose sensor was designed and validated, and then was commercially launched in 1975 [7]-[8]. The initial product was coined the YSI of Yellow Spring Instrument Company Analyzer. Ever sense this time glucose sensors have had a major spotlight leading to the concept of an implantable sensor as early as 1982, and the utilization of electron mediators for more accurate detection for point of care systems in 1984. Within the next 15 years, MiniMed launched the first in vivo continuous glucose sensor for the public. Of all the biosensor storylines, the continuous glucose monitor may be the most complete, starting from a lab in Cincinnati, to now an entirely "closed-loop" systems where the sensor communicates with a therapy device (insulin pump) and self-regulates the patient almost autonomously [6]. Using this case, one may be able to suggest the lifeline of these sensor developments, and what series of task must be accomplished to develop a sensor as mature as the CGM. This timeline begins back at 1962, where again Clarke and Lyon first described what the "modern" glucose sensor

may ensemble, utilizing the glucose oxidase as a transducer converting the chemical reaction to current which could then be measured across a cell potential. A negative potential was applied over a platinum electrode to measure the reduction of oxygen to water [6]. This method would later develop to use hydrogen peroxide as the electron carrier molecule which relied on oxygen to facilitate the transfer of electronics from the enzyme to the counter electrode and be coined the name "1st Generation Glucose Sensing" [7],[9]. A diagram for the reaction mechanism of 1st generation glucose sensors is shown below, not this is general and may have various derivative of surface chemistry, and detection method (figure 1).

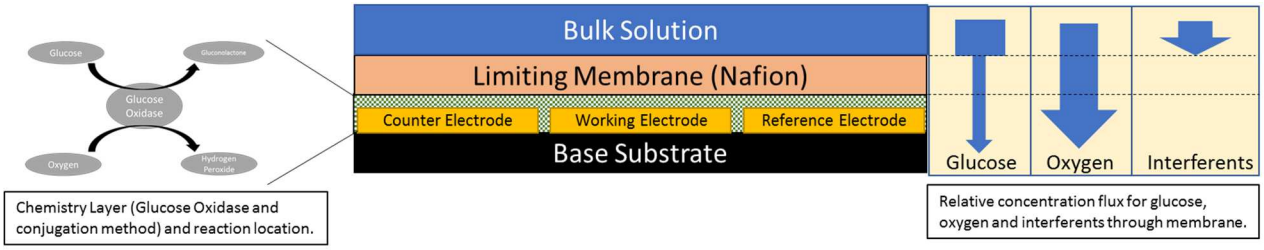

Figure 2: The image above is a high-level description of various aspects of the sensor. These include the enzymatic reaction, the general chemical deposition, as well as the flux of various molecules.

Figure 2 is a generalized depiction of a point of care, 1st generation glucose sensor. The device contains 4 main layers, first is the base substrate in which the electrodes are built on. This may be either a 3-electrode system (depicted above) or a 2-electrode system such as the Dexcom design. The next layer depicted as green shade, is the chemistry deposition layer. This may include the enzyme, and various cofactors that are needed. Depending on the substrate material, the conjugation methods may include covalent immobilization of enzymes. For gold substrate, one common example is the use of self-

assembling monolayers (SAM's) with thiol head and carboxyl tail. For graphite or carbon nanotube substrates, one common example is the use of SAM with pyrene head and NHS tail. Other immobilization principles such as biotin-streptavidin interactions can also be used. Besides covalent immobilization, chemically enhanced physical adsorption using a crosslinking molecule like glutaraldehyde can also be used.

The next two layers depict the limiting membrane for the sensor, which may be a material such as nafion (commonly used in glucose sensors) followed by the bulk solution. On either side of the main image depicts more detail such as on the left panel, shown is the electron transfer mechanism for 1st generation reactions. While on the right, is the relative diffusion amounts for the important factors in the reaction (assumed ideal). The review will go over some developments of point of care sensor chemistrys (specifically glucose sensors), these are coined 1st, 2nd, 3rd, and 4th generation based sensors. Then the development of continuous sensors will be briefly discussed including some of the algorithms and filtering methods used to both attain a clean signal and predict the signal. The final aspect will be future trends, and how this history can then be applied to the development of new sensors such as insulin.

<u>The development of 2nd, 3rd and 4th generation Point of Care Sensors.</u>

Once the 1st generation glucose sensor was developed, groups of researchers immediately began to find issues, and challenges to overcome in the design. Probably the biggest two were the dependence of oxygen to transfer the electrons, and interferents [4], [6]–[11].The dependence on oxygen leads to a major design flaw, which occurs when the glucose concentration begins to rise, and the system can no longer supply the needed oxygen to allow electron transfer. This creates an early signal saturation limit which

greatly reduces the upper and lower limits of detection. Current methods leverage glucose limiting membranes to overcome this design flaw, which prevents the total amount of glucose from reaching the electrode, while still allowing the oxygen to flow freely. This attempt to force the glucose to become the limiting factor. Although this may solve the problem under normal circumstances, there are many "non-normal" events that cause this to fail. Some of these circumstances may include exercising, or immune response where the local oxygen is up taken by other biological mechanisms.

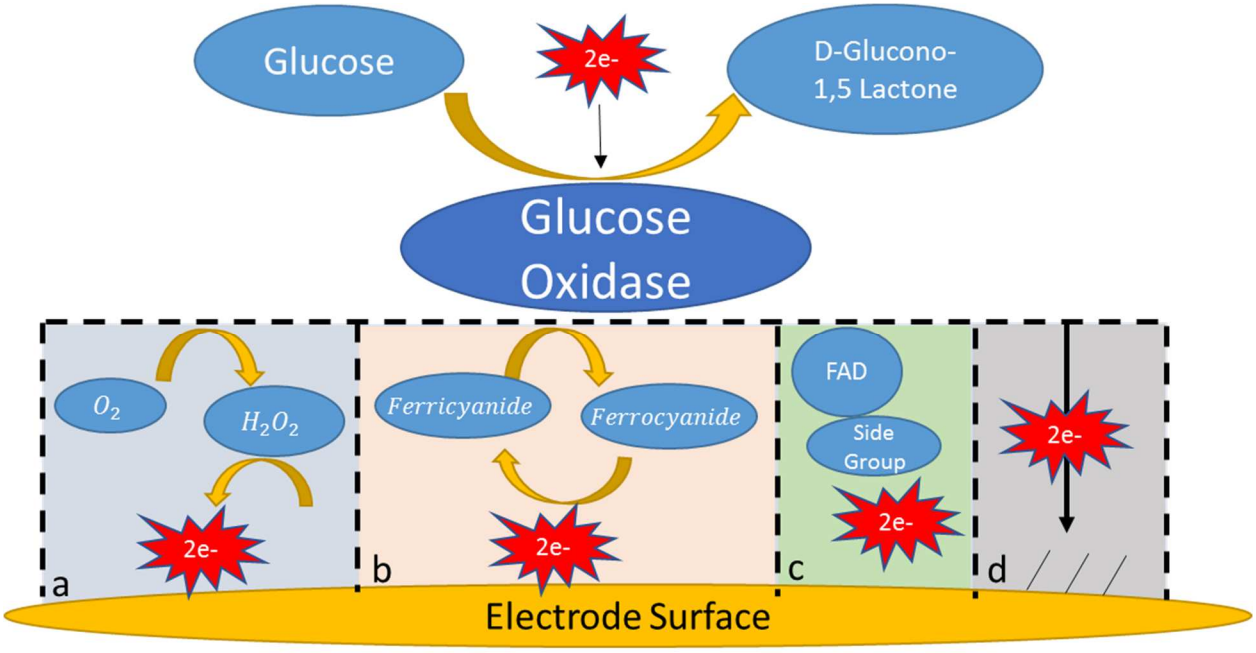

Figure 3**:** The figure above depicts glucose reacting with glucose oxidase and the various modes for electron transfer. A) First generation based electron transfer. B) Second generation electron transfer using ferricyanide and ferrocyanide. C) Third Generation electron transfer leveraging FAD and a side groups (heme). D) Fourth generation leveraging nanotubes on the electrode surface.

Simultaneously occurring to this is the interference of several other biological molecules such as acetaminophen, ascorbic acid, and other sugars [12], [13].There were several

approaches performed to improve the sensor regarding these issues. First was the introduction of electron mediators to facilitate the transfer of electrons from the reaction site, down to the respective electrode. This type of sensor is coined "2nd Generation" sensors. These electron mediators used range in design, but all perform relatively the same. Electron mediators can behave in equilibrium allowing free electrons to transfer from the area of a higher concentration to an area of lower concentration. The term electron mediator began to pop up in various articles reaching back to the 1940's [12], [13]. It became much more developed through the work from Adam Heller, who led the development of various sensors currently on the market today, including novel redox mediators, biocompatible methods of integration, and optimizing their integration in glucose sensors to improve the sensitivity and specificity [17], [17, p. 2], [18]–[25]. More specifically, Dr. Heller and his team developed a "tethered" electron mediator that can directly transfer electrons from the site of the reaction, down to the electrode surface independently of oxygen levels [23]–[27]. Furthermore, the use of electron mediators can enable the use of lower overpotentials. This in turn eliminates various interferent which may have previously been oxidized. In addition, his team developed novel redox centers that could then be formed in biocompatible methods for implantable based glucose sensors, and even worked in furthering lactate based sensors [25], [28]–[46]. This was and has been a major jump in the detection of glucose. This enabled the first types of modern point of care glucose sensors, where a patient could prick his/her finger, and within seconds receives an accurate, reliable measurement of blood glucose. The figure below depicts a traditional, second generation point of care glucose sensor developed by Abbott for Type 1 and 2 diabetics.

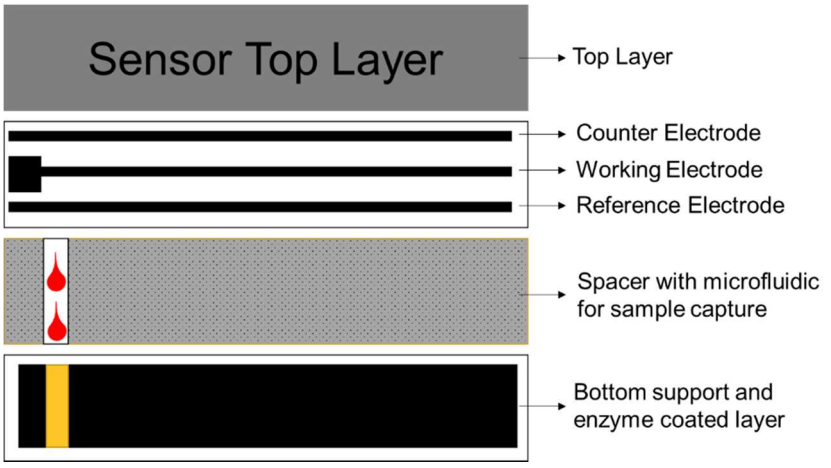

Figure 4: Typical second generation point of care sensor leveraging redox technology. The system is a 3-electrode sensor, that has an adhesive, enzyme, and electrode layers stacked in generally a roll to roll manufacturing process. Abbottt has developed a variety of derivative based on this general design with various optimization goals.

Following this research, the third generation of glucose sensing has been focusing on the mutation or alteration of the enzyme to enable direct electron transfer (DET). This mainly stemmed from the biohazards of artificial electron mediators in human body, limiting its use for *in vivo* continuous sensing. This field has broken into various interesting designs to enable the direct electron transfer. For the sake of this summary we will be focusing on the mutation of glucose, and binding of a subgroup to enable the reaction. Others have used carbon nanotubes, mesoporous carbon, as well as other surface chemistry methods that enable this direct electron transfer[47], [48]. As for the mutation of glucose or the attachment of electron mediating subgroups to enable the DET, one work worthy of mentioning is that of Dr. Sode from the School of Agriculture and Technology in Tokyo University (recently relocated to the University of North Carolina). Dr. Sode's group began looking into the use of additional side groups such as Cytochrome b562, paired with either pyrroloquinoline quinone (PQQ) glucose dehydrogenase, or FAD glucose

oxidase [49], [50]. The concept was that neither glucose oxidase, or glucose dehydrogenase could directly transfer electrons to an electrode surface on their own. This lead to the various methods described above of utilizing redox mediators, or advance micro machining of the electrode surface to enable direct measurement. The challenge of using these synthetic mediator is that many of them could not be employed in the body for long term continuous measurement, as potassium ferri/ferro cyanide, phenazine methosulphate, and quinones all have either biocompatibility issues, or at the time, challenges of tethering these molecules in a consistent manner with low variance and cost. In addition, current glucose oxidase and glucose dehydrogenase's electron mediator is bound deep inside the molecule, making access very challenging. Over a decade span, Dr. Sode's team classified both the mechanism in which electrons are transferred through FADGDH, PQQGDH, as well as begin performing various sensor designs to optimize the novel enzyme [50]–[52], such as altering the distance from the electrode using various lengths of SAM lengths.

The last generation of glucose sensing is direct oxidation of glucose without the use of an enzyme, coined 4th generation sensing. This method is heavily dependent on designing unique surface chemistry and structures that both are specific to glucose, as well as allow the natural FAD group to transfer the electron to the sensor surface. One example is the design of Graphitic carbon nitride nanosheets (g-C_3N_4NS) that were then doped with copper ions [53]. In addition, the doping of both cerium atoms, and nickel atoms were performed to better enable the electrochemical performance of the sensor, including claiming to have strong anti-interferent qualities [54]. Other methods have included molecularly imprinted electrochemical sensor (MIECS) or the use of conducting

polymers such as poly (3-aminophenyl boronic acid-co-3-octylthiophene) [53], [55]–[58]. These methods show some promise, but have not been used in industry, and seem to require significant progress to be made before the introduction into everyday use. These improvements are dependent on the surface chemistry, and process of manufacturing the enable strong reproducibility for which is required of glucose sensors. Yet, as seen in the past improvements of glucose sensing, much is derived around the alteration, or innovation of surface chemistry.

The development of continuous glucose sensor platform.

Next, the development of a continuous glucose sensor will be explored. Various designs and innovations enabled continuous sensing overcoming the challenges presented by oxygen dependency, and interference. The first major design change for a continuous glucose sensor was a reproducible surface chemistry the limited the glucose diffusion, but maximized the oxygen diffusion. To achieve this, various methods have been developed. First, we will examine the Dexcom "wired" sensor. This continuous glucose sensor is based on the use of a 2-electrode system that has a gold wire, coated in polyimide layer with a recess etched into the tip. Then, using chemical vapor deposition, various layers were applied. These include a glucose oxidase layer, glucose transport membrane layer, and a bioinert layer (such as PEG based materials). Starting with the glucose oxidase layer, a major challenge to solve was the leaching of the enzyme. This leeching caused a limit to the lifetime of the sensor, as well as challenges with reproducibility across various batches. First is the use of tethering the enzyme to the electrode as demonstrated in the Abbott Libre sensor. This method was first done in order to prevent the leeching of electron mediator's sensors, but then was applied to the same principle for enzyme

attachment to mitigate diffusion. Using Epoxy linkage, long chains interconnect the exposed amine groups of glucose oxidase down to the vinyl pyridine polymer with osmium complexes joined [59]. Once this redox hydrogel is hydrated, the osmium complexes can conduct electrons through "holes" or self-exchange in a Marcus-Type collisional electron transfer [60]. The next most common method may be the use of glutaraldehyde (GA) (or similar material) for enhanced surface adsorption. This chemically enhanced physical adsorption method was derived and optimized through many design of experiments focused on the concentration of GA, concentration of enzyme being bound, roughness of substrate being deposited on, as well as temperature, humidity, time, curing time to name a few. Even with the amount of progress made in the study and understanding of GA, there are still many unknowns and a lack of clarity on exactly how the mechanism may work. For more information please refer to Oveimar et. Al. who wrote a very detailed review on the various methods, configurations, and possible mechanisms in which GA may react [61]. For the sake of simplicity, this discussion will not go into detail on the various possible mechanisms and binding kinetics that may be involved with GA.

The next layer is the limiting membrane. This has two main uses depending on the mechanism used to transfer the electrons to the surface of the electrode. For the wired enzyme approach, which utilizes a 2nd generation method of detection, the limiting membrane serves the purpose of preventing some glucose from permeating through, as well as most of the oxygen. This is because in the case for a wired enzyme, oxygen may act as an interferent, which can create noise in the system, as well as produce hydrogen peroxide which may oxide the oxidase layer affecting the enzyme activity. As for other

CGM devices such as Medtronic's or Dexcom's sensors, the limiting membrane rejects some of the glucose, but allows the oxygen to diffuse in excess. The general design is proprietary, but consist of a polyurethane polyurea block copolymer which is a mixture composed of various materials such as; hexamethylene, diisocyanate, aminopropyl-terminated siloxane polymer, and polyethylene glycol. For this design, the oxygen is easily permeable through the siloxane material, while glucose only partially diffuses due to the hydrophilic diol group . Abbott uses a proprietary vinyl pyridine-styrene copolymer with an epoxy group. This is then functionalized with various side groups to improve the biocompatibility for the system, even being demonstrated to last over 1 year in rabbits with little to no encapsulation [62]. The last layer added is a bioinert layer that will be in contact with the body to help minimize immune response and other unwanted interactions. This generally makes up what a CGM will look like with various alterations based on the company, and proprietary information. The next development in the path to a continuous monitor where the predictive algorithms, software, and hardware required to enable such technology. For the sake of this discussion, these topics will not be described during this writing.

Current Sources of Error in Glucose Sensors:

This history of glucose gives a strong depiction of the timeline, and stages for a biosensor. There has also been large amounts of work involved with classifying error regarding these glucose sensors. In general, there are many factors that may affect a reading output by either the point of care sensors or CGM. Sensors are rated according to their precision and accuracy. Precision being the reproducibility of the sensor, or manufacturing process, and the accuracy being how close any one reading is with respect

to the reference measurement. The current gold standard for depicting both accuracy and precision is by plotting the measured value in the y-axis, against the reference value in the x-axis. This graph can be presented in either the Clark Error Grid, or the Surveillance Error Grid. In the Clark Error Grid, majority of the data points should ideally fall within zone A, which shows that the measured points are within 20% error of the reference methods. The Surveillance Error Grid is a more visual version of Clark Error Grid developed recently by Dr. Klonoff [63]. It converts the error into risk levels and present them in a color-coded manner.

The difference between the measured values and reference values are known as errors. While there are multiple ways to express errors, such as the coefficient of variance, with the emergence of CGM, MARD (mean absolute relative deviation) has gain popularity as it is capable of summarizing the accuracy of a CGM over a period of time in a single value [65],[66]. It is typically obtained using data from clinical trials by computing the difference between the CGM measurements and the values that are simultaneously measured by a reference system. These error values are heavily valued by FDA and ISO to develop the standards for blood glucose meters. Following this in 2003 the International Standards Organization worked with a plethora of health providers, and government agencies to develop the ISO 15197 which stated the following (ISO standard):

1) 20% of glucose values above 75 mg/dl
2) 15 mg of glucose values below 75 mg/dl

This has recently been updated in 2016 with tighter controls. A summary of important values is described below:

1. 90% of glucose values within 5% error of reference for blood glucose below 75 mg/dl
2. 80% of glucose values within 5% error of reference for blood glucose equal, or above 75 mg/dl

For more detailed information please refer to the full FDA report, or the executive summary [65], [66].

Various other groups have advised tightening these controls including the American Diabetes Association (ADA) suggesting that 95% of glucose readings be within 5% of the reference value. There are a multitude of factors which affect the error of these devices. Strip to strip error can occur through the size variation of the well shape, as well as variance within the amount of enzyme applied. Most test strips use excess enzyme to avoid the error caused by slight under application or variation [67]. Although the thinning of the enzyme will not affect the glucose reading greatly, bare spots may result in large underestimation since most algorithms relate to the functional surface area. The next source of variation comes from variance in the electron mediator. Normally the reactions occur and the transfer of electrons flows from the glucose, to the enzyme and is carried to the electrode by an electron mediator. If there is a shortage of electron mediator, the mechanism will change, requiring the presence of oxygen to enable this transfer. Immediately, the measurement errors will increase as the sensor then relies on the environmental oxygen levels which can vary within the sensing system. Oxygen in addition is a major source of variance due to its competitive nature with the electron mediator for electrons. This mediator may also be affected by the temperature, and stability over time. Both of which may result in an increase of error [68]. Patient factors

are also key and can impose great variance on the system [67]. Other patient factors include washing their hands, or not up taking enough volume (although with the use of microcapillaries this has been greatly improved). With all the room for error, and miss-use of both point of care, and continuous devices, various filters, and algorithms have been employed in attempt to help overcome this weakness.

Continuous Glucose Algorithms, Calibration, and filtering aspects:

There have been many review articles on the design of glucose sensors, ranging from chemistry, to the transduction method, as well as various clinical studies of their efficacy. One characteristic that receives much less attention are the calibration algorithms, and methods of filtering the raw signal coming from the device. These algorithms are used for various reasons, such as predictive modeling for hypo/hyperglycemia alarms, lag time between the signal glucose and current levels, as well as filtering the raw signal into a manageable curve [69]. Typically, a linear regression calibration curve is applied for the detection of glucose:

$y = mx + b$ Eq. 1

Where y represents the current signal and x the corresponding glucose pair. This equation must then be calibrated to find a relation to the blood glucose from the interstitial glucose levels which is essentially the slope (m) of the curve. This then takes the form:

$m = \frac{y-b}{x}$ Eq. 2

Using a linear regression method as the one described above assumes that the independent variable is known, and that the dependent variable is uncertain. Past studies, such as those from Panteleon, and Ginsberg ([67],[70]) have shown that using the glucose

signal as the independent variable improves the signal. This then flips the equation to be as follows:

$$x = my + b + e \qquad \text{Eq. 3}$$

Where e represents source error, and variance from the calibrated reading to the predicted reading. Once given a calibration, the system then will use a technique of minimizing the sum of the squares (or similar method) to attempt and eliminate the difference in reference value to the calculated values. This takes the equation of:

$$\min_{m,b} \sum_{i=1}^{N} e^2 = \min_{m,b} \sum_{i=1}^{N} (x_i - x_{cal})^2 \qquad \text{Eq. 4}$$

Where i is the specific data point, N is the total number of previous points, with the goal of minimizing error (e) while controlling the slope and y-intercept (b) ([69]). One other major challenge with calibration is the time in which a patient calibrates his/her sensor. A group called DirecNet Study characterized various noises introduced to the calibration method leveraging Medtronic CGM's, finding that accuracy quickly degraded when the sensors are calibrated during a rapid change in glucose (about 1.5 mg/dl/min or more). This suggest that for optimal calibrated, a steady state current, or glucose value would be beneficial as the best correlation between ISF and blood glucose occurs during steady state periods.

The next aspect is filtering the data being input, which various common filters being used. These are finite impulse response filters, infinite impulse response filters, Kalman filter, and wiener based filter. Medtronic has patented a weiner based filter where the parameters of a finite impulse response filter are found by minimizing the sum of the squares error between the signal and the reference value applied. The next important filter is the Kalman filter which is considered superior to the weiner based on a few

research teams work ([69], [71], [72]). The Kalman model switches between the prediction value based on statistical certainty based on time-varying events ([69]). Depending on the strength of the model, the Kalman filter can achieve stronger glucose relationships for ISF to blood, as well as strong predictive analytics. Dimitri Boiroux et al performed a comparison of various Kalman filter methods such as least squares estimation, Huber regression, and Gaussian maximum likelihood ([73]). The results of this study showed that the Gaussian maximum likelihood method achieved best results, as well as enabled the ability to include uncertainties from various errors, or from population based models. The strong drawback was that this method did require the most time to compute the outcome of an event. As powerful as these filters, and linear regression techniques are, there is still excessive amounts of information that is lost, or disregarding. These include the integration of various metabolic models to help better predict future glucose values. These models, such as Medtronic's virtual patient, can help validate, and further allow for predictive decision making. Furthermore, the integration of Bayesian methods for risk and uncertainty of predicated values may enable better outcomes, as well as enable the ability to better design for population based data as previously mentioned.

Future Trends:

Glucose sensors have a vast history, which has led to the development of tremendous therapy's, and treatment methods for diabetics. Still, there is much room for improvement, and progress in the field as well as adjacent fields in which the technology rely upon. These include the development of novel surface chemistry technique which both improve the signal transduction methods, but eliminate noise caused by the

environment. In addition, technologies in the field of computer science are becoming more relevant and applied to everyday systems. The use of machine learning, and artificial intelligence has vastly improved many fields including supply chain management, manufacturing reliability, and design process ([74]–[77]). This same technology is also starting to be leveraged in diabetes treatment, developing individual based treatment and therapy that are specific to each patient. This is being implemented already in the type 2 diabetes market as recent work employing machine learning has begun to categorize the disease sate as 5 separate diseases versus the 2 commonly believed today ([78]). Organic solutions have also become more prevalent, as the University of Washington demonstrated the integration of a co-polymer with beta-cell transplant to help prevent immune rejection of the tissue ([79]). Simultaneously, there are new pharmaceutical drugs being developed and tested constantly improving the outcomes of patients. In more recently industry, both Abbott, and Medtronic have made several leaps towards next generation therapy. Medtronic has begun to pave the road with the releases of the 670G insulin pump which not only communicates with a continuous glucose sensor, but also can adjust some patients basal according to the value ([80]). Simultaneously, Abbott has released the first calibration free sensor titles “Libre” which is factory calibrated meaning that patients do not need to calibrate the sensor by using a glucometer ([81]). Interestingly, each innovation was done for a separate market. The Libre sensor development was done for type 2 diabetes, while Medtronic’s innovation was aimed toward type 1. Other startup companies have begun to appear developing major increase in technology. One is called Beta Bionic who has worked with various technology groups to develop the first dual hormone treatment pump ([82]–[84]). Most

research showed the various challenges with such a device, 1 being the stabilization of glucagon (a hormone which signal the liver to release glucose when the blood sugar drops to low). Another major development is the algorithm utilized to predict how each hormone should interact, and be used. Giving the device complete autonomy greatly improves the patient compliance and outcomes, but may also pose a tremendous threat if a misreading or mistake should occur. This risk leads to the last major technology improvement, which is increased accuracy within the CGM devices. In late March of 2018, both the Dexcom G6 was approved by the FDA as the first calibration free sensor aimed towards type 1 diabetics, as well as Senseonics receiving FDA approval for a 90-day implantable continuous sensor. Both are major innovations in the goal of designing an autonomous artificial pancreas ([85]).

CHAPTER 2

DEEP DIVE INTO INSULIN PUBLICATION AND KINETICS OF INSULIN MRE'S

Current understanding of the kinetics of insulin, and anti-insulin are based on a series of experiments performed to measure the equilibrium constants, both as binding occurred, or at equilibrium state to attempt and validate. These studies have shown Scatchard analyses with concavity's like interactions that represent when 2 affinities of binding sites are present. By this, we mean that one of the binding sites has high affinity, and another site has much lower affinity od the same molecular recognition element ([86], [87]). This creates challenges when attempted to model this interaction as the simple antigen + antibody reaction. In addition, this begins a more non-linear function. The interesting aspect is that insulin has been shown to show both positive cooperativity, and negative depending upon the concentration ([87]–[92]). There are many possible reasons why this may be the case, first, there may be dimerization issues when the concentration of insulin increases. In addition, as the concentration of insulin peaks, steric hindrance may begin to increase the dissociation constant. Another concept may be that this relates to the differential binding affinities of the antibody. At low concentration, all the high affinity sites bind rapidly, but as these began to saturate with the increase in concentration, the low affinity sites began to bind.

Insulin was previously studied in Dr. LaBelle 's lab utilizing electrochemical impedance spectroscopy. The goal was to fabricate a proof of concept for a point of care insulin sensor. The work had many challenges, as the team altered various pH levels, concentration of antibody, and very interesting results came from this. The most interesting aspect was the appearance of two different frequency peaks. To improve the

sensor, we averaged the two peaks together and designed a calibration curve accordingly. The figure of this is shown below:

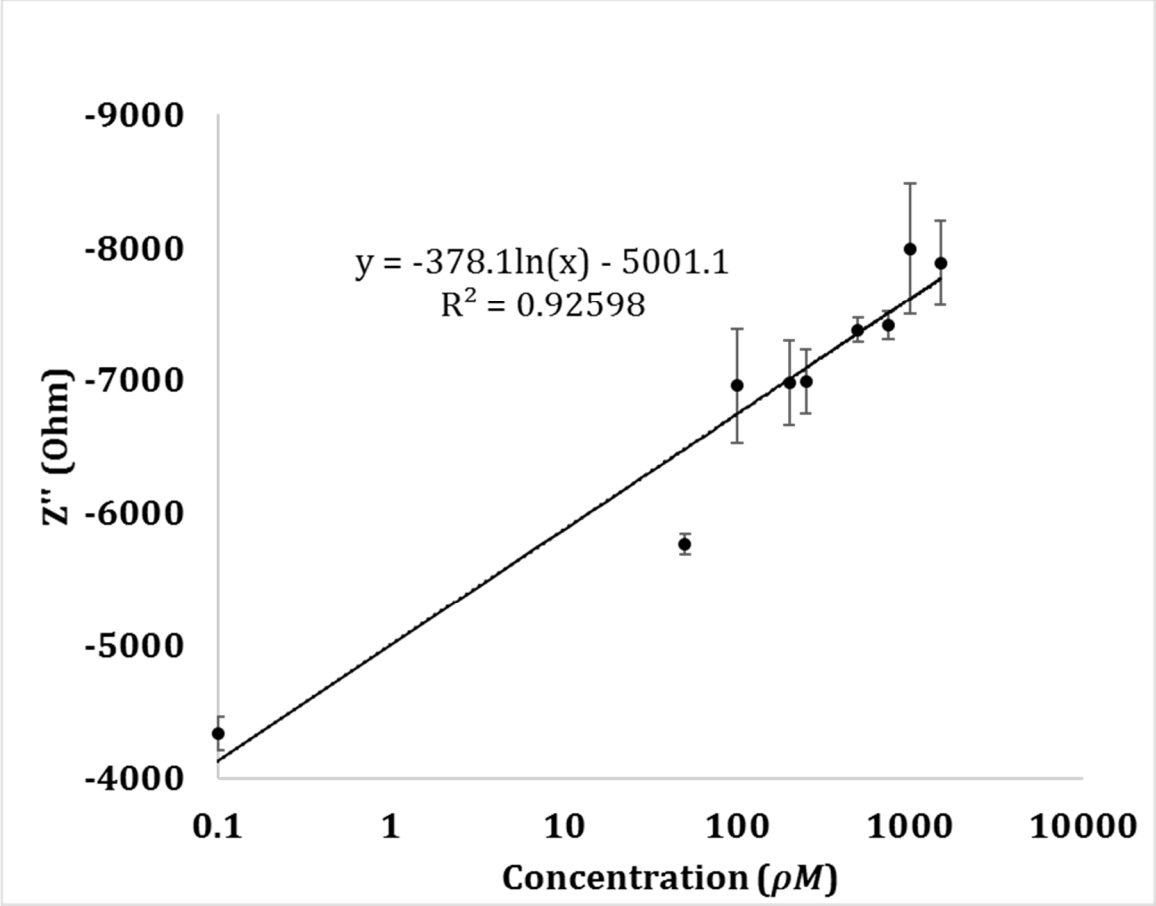

Figure 5: The of a calibration curve of 0, 50, 100, 200, 250, 500, 750,1000, 1500 ρM based off imaginary impedance readings of insulin based on the initial study done in lab. This was measure at 810.5 Hz, which the team derived of the two following curves:

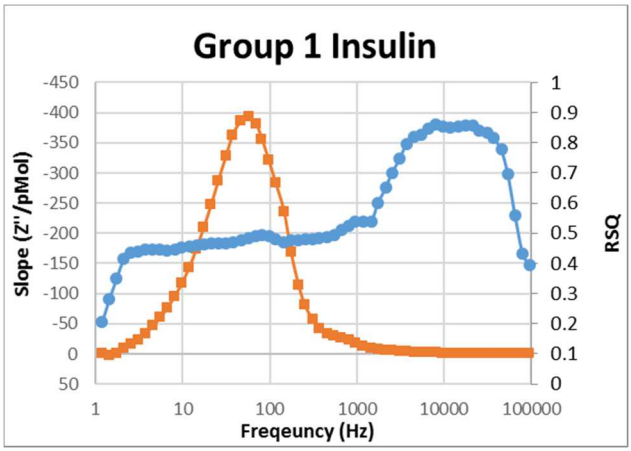

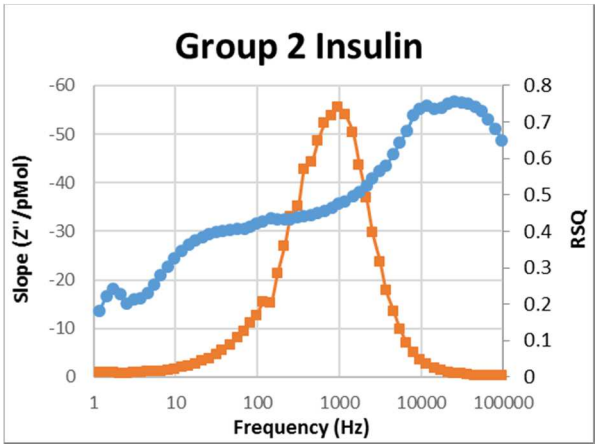

Figure 6**:** The two graphs above represent the two-binding frequencies measured using the insulin sensors. One is much lower, and the second is much higher, this is attributed to the two binding sites, and the distribution of binding.

The figures above show some of the complexity which was seen when attempting to detect insulin. There are various theories built around why this observation occurred, first was the idea that insulin has two differential binding sites. Each with different affinities, and based on the concentration make interact differently. This was then further researched, to find that not only are there two binding sites, but insulin as interact laterally with adjacent antibodies. This phenomenon makes the detection very challenging, as there is noise added to the system. The analysis then went to see if a

circuit fit would improve on the system, began to understand the electrical relationship with each peak, as well as the combined spectrum. The model use was a modified Randel's circuit. "Using the system geometry and the results of the electrochemical circuit modeling, an imperfect parallel plate capacitor (IPPC) is used to model the interaction of chemical and biological molecules. The surface of the sensor is considered as the bottom plate. The molecular recognition elements and the bounded target molecules at the end of the SAM are considered as the top plate of the capacitor. The length of SAM chains determines the distance between the two parallel plate capacitors. While the bottom plate is relatively smooth, the top plate, depending on the orientation of the MREs and the binding of target molecules, can report varying degrees of surface roughness" ([93]). This same concept described by Dr. Lin is seen in the circuit, and calibration curve below:

Figure 7**:** The above circuit is a modified randel's cell. Q, represents constant phase element which is has been commonly used to represent an imperfect capacitor. The two resistors represent the electron transfer, and solution resistance.

Figure 3 can be broken into a few equations, generally the constant phase element (Q) is of most interest.

$Z_{CPE} = \frac{1}{Q(j\omega)^n}$ Eq. 1 ([94])

The equation above is the representation of the constant phase element. Where $j = (-1)^{\frac{1}{2}}$, $\omega = 2\pi f$ with f being the frequency of the applied AC potential, and n representing a fractional value between 0 to 1, with 0 describing a pure resistor and 1 an ideal double layer capacitor [88]. There are various relationships between the constant phase element, and the surface. This was seen also in the data collected, as the two-different impedance peak location also correlated to different n values. The lower peak being must lower in value then the higher suggesting that the surface was either more rough, or dynamic, creating a less than ideal capacitor in the parallel plate. The relation may be due to the different binding affinities of the two IgG sites. Effective capacitance (C_{eff}) is then related to CPE, derived from [95], [96] as a method to estimate what the ideal capacitor would look like:

$C_{eff} = Q^{\frac{1}{n}} * \left(\frac{R_S R_C}{R_S + R_C}\right)^{\frac{1-n}{n}}$ Eq. 2

Using this process, the two groups effective capacitance was analyzed and the following curves where reported:

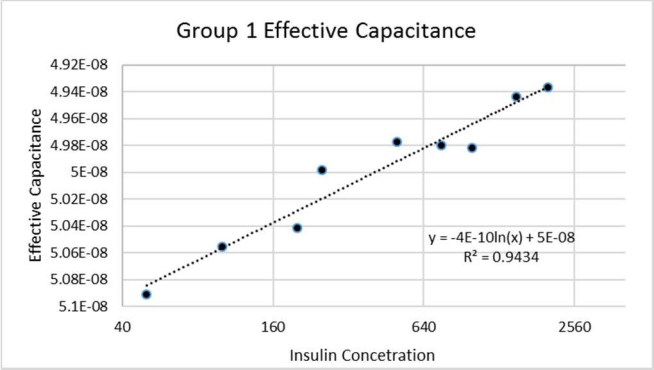

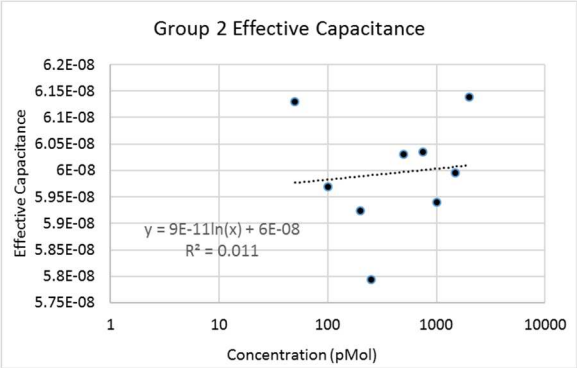

Figure 8**:** The two figures above represent the 2 different groups, but organized by effective capacitance instead of the frequency peak. Interestingly there is very clear correlation in group 1, which is represented by the lower frequency range. Whereas group 2 has very little to no correlation.

This data shows a very interesting aspect, that the two groups showed very different characteristics. The electrode analyzed came across 15 different experiments and where scattered throughout the different test. In addition, the lab performs a post-MHDA measurement which is used as a quality control for the lab. Nearly all of these electrode across both groups (1 and 2) had normal baseline MHDA impedance spectrums, and where tightly batched. This process was done through the following protocol taken from Malkoc et al. “Electrodes were prepared in batches of eighteen and all electrodes were analyzed using EIS. After measuring the post-MHDA impedance, the quality control

(QC) was executed by selecting only the electrodes with similar peak frequencies and impedance magnitudes that are within 6% to 10% relative standard deviation (%RSD). Only the QC passing sensors would then proceed with immobilization." Malkoc et al. This further suggest that the variance is seen in the next stages of the conjugation method. This is also refuted through the detection of the blanks, which is the second quality control which showed similar results across the batches. Due to these quality control methods, the only aspect left to create such a difference is the mechanism of binding. Through all of this work, the lab realized that a better understanding of the mechanics for insulin interaction with the receptor must be understood. To do this I present a small overview of the all the work that has been done, and the current thoughts and understanding of the process.

Measurement of the Affinity of Antibody – Antigen Interactions basic example (insulin Example)

Affinity: The detectability of a specific target biomarker

Specificity: The relationship between the amount an antibody binds to a target versus non-target molecule.

Affinity can be defined in two methods, first is through kinetics, and the second is by thermodynamics. We will go through both for a basic example of insulin and anti-insulin interactions.

Insulin: I

Anti-Insulin: AB

Complex: IAB

Ka: Association Constant

Kd: Dissociation Constant

[I], [AB], [IAB] → Respective concentrations

$AB + I \overset{K_a, K_d}{\longleftrightarrow} IAB$ Eq. 1

First, at equilibrium, both the association reaction, and dissociation reaction will exist at equal rates (the amount of insulin binding is equal to the amount of insulin unbinding) as seen in equation 2 below:

$K_a[I][AB] = K_d[IAB]$ Eq. 2

The affinity constant K, is defined as the association divided by the dissociation constant. Using this to solve equation 2 we get:

$K = \frac{K_a}{K_d} = \frac{[IAB]}{[I][AB]}$ Eq. 3

This is the basic kinetic model, which is governed by mass action.

Next, the basic thermodynamic model will be explained, and expressed. This assumes that K, is determined by the amount of total free energy changed within the system being interrogated (also assume standard conditions and steady state with 1 Mol reacting)

$\Delta E = -RTln(K)$ Eq. 4

R is the gas constant, T is the temperature. This suggest that if there is a change in free energy of the system, the affinity will also change. Addition of side charged groups may prove beneficial when trying to "control" this binding and affinity.

[AB]t: total concentration of antibody available

n: Number of "active" binding sites available on the antibody.

Before going further, let's take a quick side walk down the path of how antibodies are designed, and structured….

Assume the anti-insulin is a IgG anti-body structure. In general antibodies are made up with heavy and light segments which may be referred to as “domains” in which the interact with the surrounding environment. These are related to a broader family of molecules coined “immunoglobins” (Ig). The heavy chain makes up for about 60 kDa of the weight, while the light chain can make up for about 25 kDa. Traditionally, these Ig’s consist of a pair of light chains, and heavy chains that are structurally symmetrical in design. This design has the shape like that of a Y, with a light chain covalently bound to a heavy on one side, then a symmetrical light and heavy chain bound on the left, interconnected by various disulfide bounds. In physiological environment, these molecules serve various duties, from recognition, to activation, and inhibition to name a few. But in the use of a sensor, only 2 aspects are of interest, first is the recognition (or specificity to a target) and the second is affinity (how well the target binds). IgG’s specifically contain 1 unit, with 2 valence binding sites. Simply put, for each antibody, there are 2 binding regions available. In an ideal sensor, these antibodies would be immobilized to the surface (see Immobilization section), and then be activated ready to bind when the target molecule is applied. This method of application using immunoassays (most famously ELISA) have led to the design of very specific antibodies that bind for very long periods of time. This poses a challenge for the goal of a continuous sensor, which is being able to measure a decrease in concentration. Since most antibodies have very high affinity constants, this means that it is much easier to add

analyte, then remove it from the system. Shown below is a graphical example of what is being discussed:

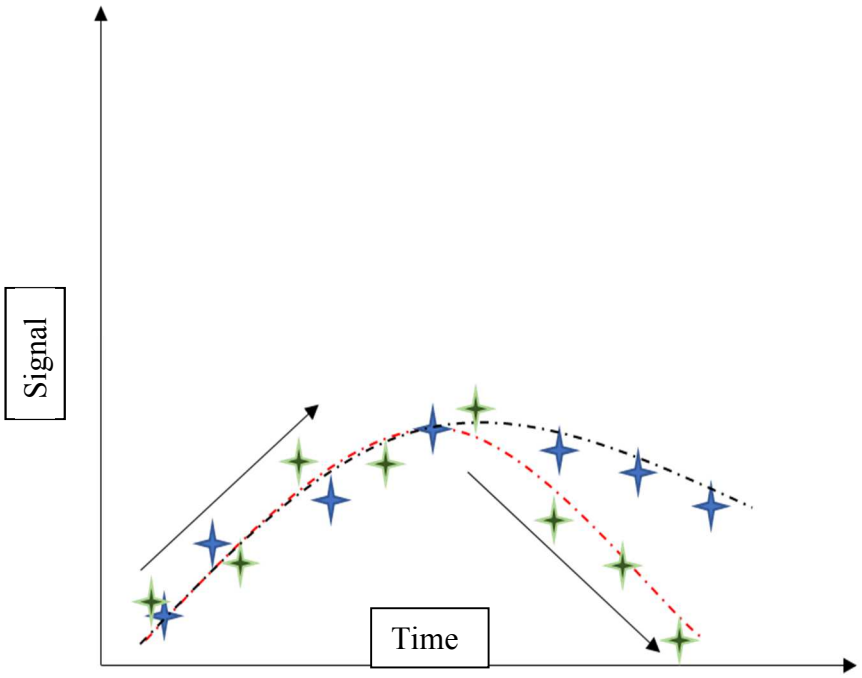

Figure 9: The image to the left depicts the time, versus the change in concentration. The light green is enzyme based, whereas the blue is antibody based. The dotted lines represent the trend lines which the signal output may look like, while the stars represent the actual concentrations in the sample.

This challenge is one of the major reasons that antibody based assays have been limited in use for continuous based sensor platforms.

Now, coming back to the simple thermodynamic model, we can assume the insulin antibody is an IgG with 2 valance binding sites. One important aspect to note, is that these sites do NOT have symmetrical binding affinities, in addition, the molecule once bound to a single site, may "conform" over to the second site.

Let Mr be the molar ration of bound insulin/Antibody for the system. Using this, we then get the equation as follows:

$$Mr = \frac{[IAB]}{[AB]_t} \rightarrow [IAB] = Mr * [AB]_t \text{ Eq. 5}$$

Taking this, and noting that the free antibody sites is equal to the total amount of antibody, minus the bound concentration of the complex:

$[AB]sites = n * [AB]_t - Mr * [AB]_t \rightarrow [AB]_t(n - Mr)$ Eq. 6

Let the unbound insulin: I_{un} and use these new assumptions to show the following relation:

$K = \frac{[IAB]}{[I][AB]} = \frac{Mr*[AB]_t}{[AB]sites*[I]} = \frac{Mr*[AB]_t}{[AB]_t*(n-Mr)*c} \rightarrow \frac{Mr}{(n-Mr)*c}$ Eq. 7

Equation 7, basically helps provide both the relationship between the affinity and the molar ration bound, with the concentration of insulin, and number of valence sites. In addition, this demonstrate how the affinity is partially related to the amount of available insulin to be bound, suggesting that it may have slight dynamics. Furthermore, may be utilized as another method to find the affinity through different test, such as Langmuir, or Sips plots.

The next important factor to binding kinetics is the binding association, and dissociation which correlates to the time constant of the interaction. From a structural view this all depends upon the geometry of the molecule, closeness of fit, and charge of the interaction. The association constants for most antibodies are generally similar, ranging from around 10^7-10^9. The dissociation constant has much larger variance, ranging from 10^{-4} for higher affinity's, up to 10^4 for very poor affinity. The half-life of the reaction is related to the dissociation constant through the following equations:

$\frac{d[IAB]}{dt} = -K_d[IAB] \rightarrow \frac{d[IAB]}{[IAB]} = -K_d dt$ Eq. 8

$Ln[IAB] + c = -K_d t$ Eq. 9

$c = -Ln[IAB] \ at\ t = 0$ Eq. 10

$$Ln\left(\frac{[IAB]}{[IAB]_0}\right) = -K_d(t - t_0) \quad \text{Eq. 11}$$

When you set time to ½ for the half-life of the binding interaction. Plugging this in we then get the following equation:

$$t_{1/2} = \frac{.693}{K_d} \quad \text{Eq. 12}$$

The half-life is the time in which the reaction take place. For a high affinity react the half-life may be up to 19.25 hours. This is very good for immunoassays due to the need for specific and strong binding, but for a continuous sensor this creates a very impractical design.

CHAPTER 3

MODELING AND OPTIMIZATION OF BINDING KINETICS

This is an incredibly over simplified case for many reasons; first is that insulin has 2 binding sites being an IgG, each of which have different binding affinities to insulin. Furthermore, once bound to a single site, lateral interaction may occur (binding from 1 site, laterally to the next site) from one antibody to the next, or within the same antibody from one valence site to the other. In addition, the complexity of how the antibody is immobilized must also be considered. Assuming close packaging is a simple way to greatly ease the process, but still should be considered. The amount of impact these may have are directly related to the affinities of each site. Below is a figure depicting the various interactions of importance (excluding surface chemistry of self-assembling monolayer) ([67], [87], [97]–[99]).

Assumptions:

1) Antibody is an IgG with 2 valence binding sites with different affinities
2) I_1AB is the concentration of Valence site 1, bound with antigen
3) I_2AB is the concentration of Valence site 2, bound with antigen
4) AB_u is the unbound antibody
5) I is the amount of available insulin near the surface
6) I_B is the concentration of insulin in the bulk solution
7) The system is well mixed
8) Close packaging for surface immobilization of antibody
9) The antigen can move "laterally" from valence site 1→2, and from 2→1 within the antibody and between two adjacent antibodies.

The figure below depicts the various interactions that may occur with the antibody-antigen system.

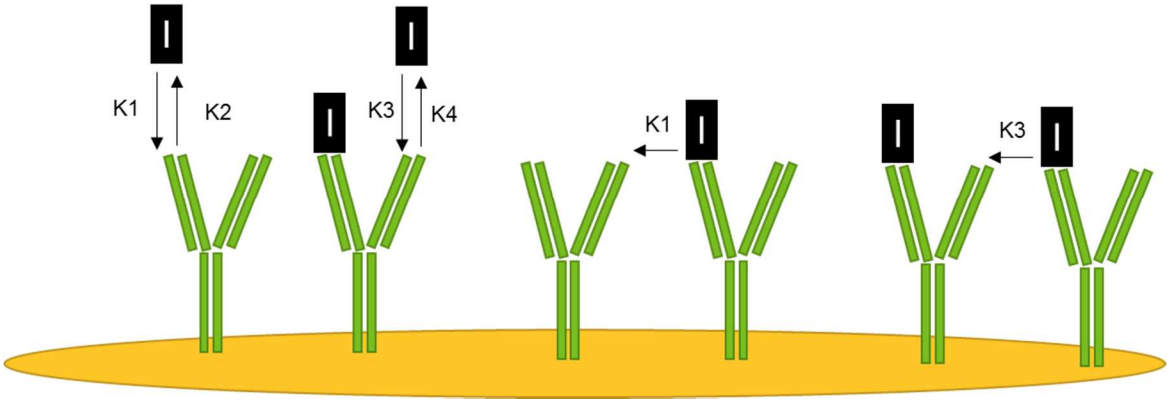

Figure 10: The figure above shows the various binding interactions that may occur with the antibody-antigen system. The black circle 1,2 represent the 2 binding sites, while the various "K" values are the binding affinities for respective reactions. Note: each K is NOT the overall affinity which is the association over the dissociation.

Using the assumptions, and figure 5, we can attempt to build more realistic rates of binding and unbinding of the various molecules. (refer to drawing)

$$\frac{dI_1AB}{dt} = K_1[AB_u][I] - K_{-1}[IAB] + K_{-2}[I_2AB] - K_2[IAB][I] - K_3[AB_u][IAB] + K_{-4}[I_2AB] - K_4[IAB] \quad \text{Eq. 13}$$

$$\frac{dI_2AB}{dt} = K_2[IAB][I] - K_{-2}IAB_2 - K_{-4}[I_2AB] + K_4[IAB] \quad \text{Eq. 14}$$

$$\frac{d\mathrm{I}}{dt} = K_{-1}[IAB_1] - K_1[AB_u][I] + K_{-2}[I_2AB] - K_2[IAB][I] \quad \text{Eq. 15}$$

$$\frac{dAB_u}{dt} = K_{-1}[\mathrm{IAB}] - K_1[AB_u][I] + K_3[IAB] \quad \text{Eq. 16}$$

This is a divalent receptor model, which is one step more complex than the traditional antibody-antigen reaction kinetics. There are various factors here which we can control to help improve the continuous platform of the system. These include the concentration of

antibody bound to the electrode, as well as the amount of antigen "allowed" to reach the surface of the electrode. These values will not be constant, in fact, they will most likely fit into a distribution function of concentration bound to the surface. The goal would be to optimize the concentration on insulin antibody on the surface which will increase the dissociation constant to a point at which continuous detection would be possible. The goal would be a time constant of lower than 30 minutes if possible, while still have the resolution to measure small changes in insulin (pmol). The proposed method to do this will be to model the system of differential equations as either normal or beta-distribution functions. For simplicity, we will assume that all the distributions are normal and can't be negative.

This is a brief introduction to the basic method in which antibodies interact with antigens. It is important to note that in an unideal system these are vastly inadequate to describe the system. To overcome this the use of Matlab have been applied to better understand the system and interrogate the design.

The parameters ran for the Matlab program were assuming various concentrations. Antibody started at 1 uM of concentration, and was tested both an order of magnitude above, and below. This was tested against a gradient of insulin concentrations to see how the effect of changing concentration changed the amount bound vs free. The outputs analyzed were the following: Sensitivity which is defined as the lowest amount which is bound. The change in equilibrium, with respect to change in concentration. This was looked at to measure the expected change for continuous detection. Other calculations performed were the binding half-life, as this is less in our control due to being related to

the dissociation constant. To model test was to run various concentrations until equilibrium was reached. Once equilibrium was obtained, this was then set as the new initial condition for the next iteration. The concentrations were 50, 250, 500, 750, 1250, 2500pM. After that increase, the final parameters of 2500 would be set as the initial condition and the concentration applied would be back to 0. The code used was derived off Dr. Caplan's binding model, as well as another code altered from a Michaels Menton interaction.

To simplify the model I focused on simply modeling a bivalent interaction (2 binding sites with differential kinetics). Dr. Caplan helped design the used matlab code. In addition, I attempted to model a more complex version of the kinetics using the effect of lateral interactions. The results and code of the first, simpler model as shown below:

```
function yp = InsulinAbrhs (t, y, p);
Ib1=y(1); Ib2=y(2);
yp=y;
Iu = p.Itotal - (Ib1 + Ib2);
Au1 = p.Atotal - Ib1;
Au2 = p.Atotal - Ib2;

%Insulin bound to antibody site 1
yp(1) = p.ka1*Au1*Iu - p.kd1*Ib1;

%Insulin bound to antibody site 2
yp(2) = p.ka2*Au2*Iu - p.kd2*Ib2;
```

```
p.ka1=1e5;

p.kd1=9.9e-4;

p.ka2=1e5;

p.kd2=1.299e-1;

p.Atotal=9.178e-6;

p.Itotal=0e-9;

p.Vr=100;

p.Ib10=4.956606e-8;

p.Ib20=3.801558e-10;

p.tf=1000;

y0=[p.Ib10 p.Ib20];

options = odeset('AbsTol', 1e-10, 'RelTol', 1e-7);

[t y] = ode15s(@InsulinAbrhsTake2, [0 p.tf], y0, options, p)

InsulinBound = y(:,1) + y(:,2);

figure(1);

plot (t, y);

xlabel ('Time'); ylabel ('Insulin bound'); title ('Insulin binding');
```

The above code provided and altered by Dr. Caplan was used to test a half-factorial design of experiment built on minitab. The chart below shows the variation in parameters and the type of factorial ran:

Test Number	Antibody []	Kd1	Kd2
1.00E+00	1.00E-07	1.00E-04	1.00E-03
2.00E+00	1.00E-06	1.00E-04	1.00E-02
3.00E+00	1.00E-07	1.00E-05	1.00E-01
4.00E+00	1.00E-05	1.00E-05	1.00E-03
5.00E+00	1.00E-05	1.00E-03	1.00E-01

Table 1: The half factorial DOE tested with the parameters of dissociation constants, and antibody concentration. The association constant was left at 1e-5 to keep high sensitivity.

Each group of settings was tested against the described gradient of insulin above, and the outputs where time of dissociation, as well as the "best fit". Currently this is being performed through visual interpretation of the graphs, but other methods may also be of interest.

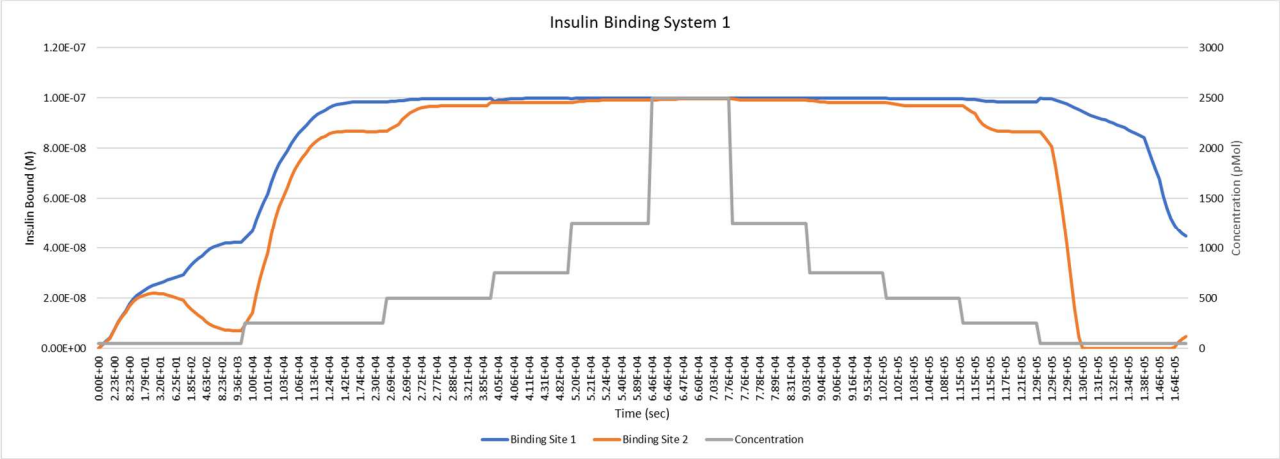

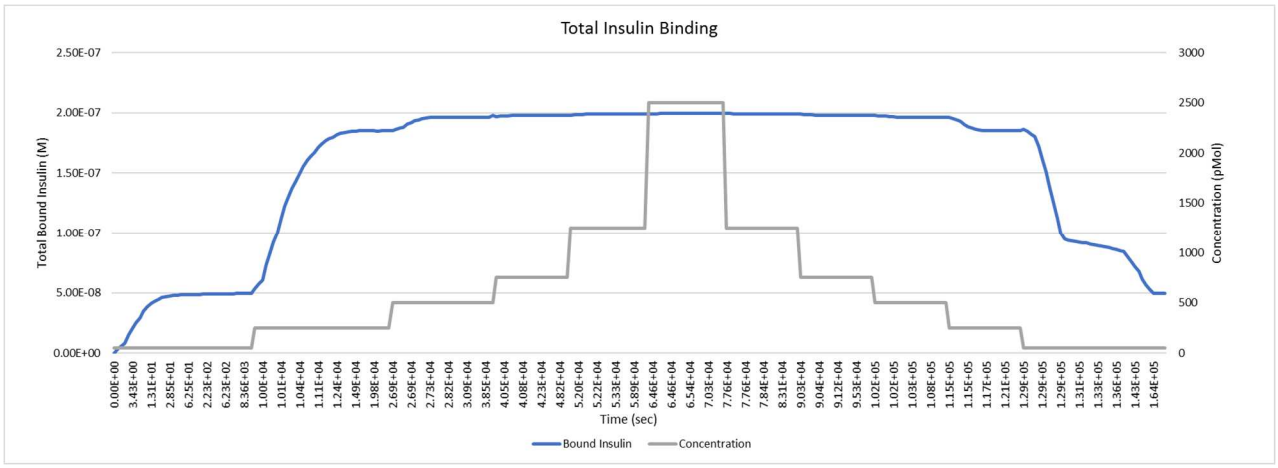

Figure 11**:** The above figures are the concentration fluctuation and the binding affects as seen with settings 1 of the half factorial DOE. The specific settings of the model are shown above.

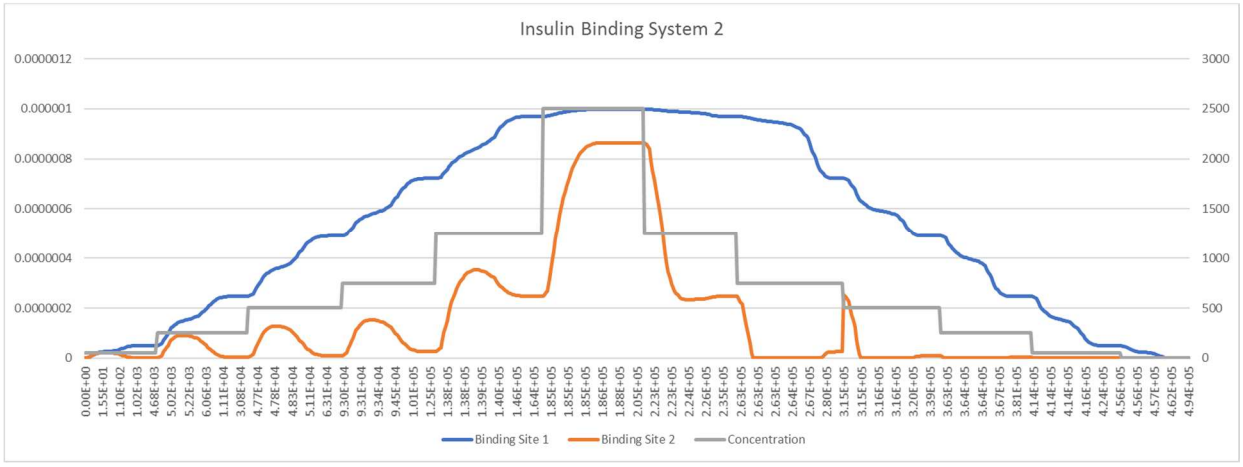

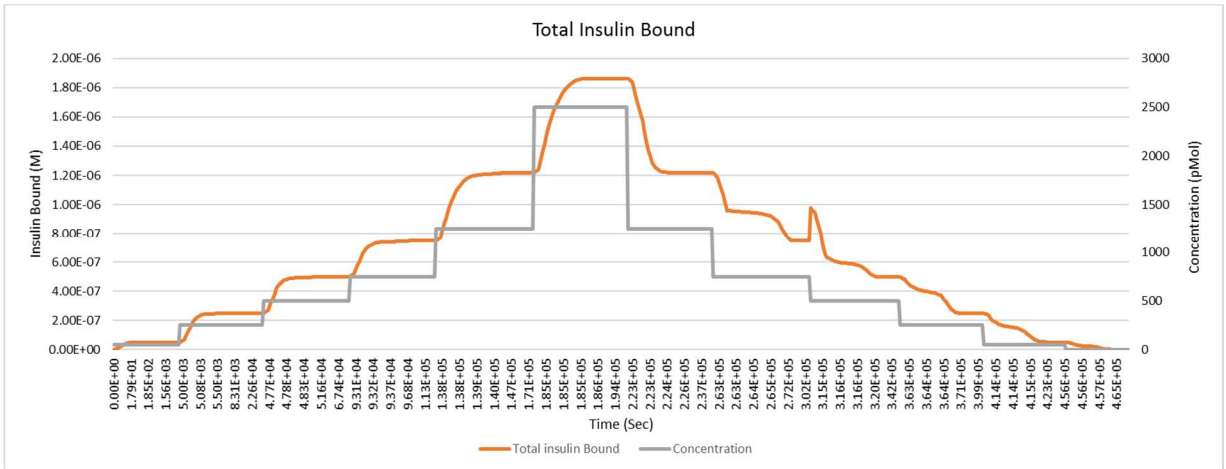

Figure 12: The above figures are the concentration fluctuation and the binding affects as seen with settings 2 of the half factorial DOE. The specific settings of the model are shown above. Note that for binding site 1, there is a sudden change in binding, but then the signal quickly deteriorates. The total binding curve (addition of site 1 and 2) resembles a much-improved fluctuation.

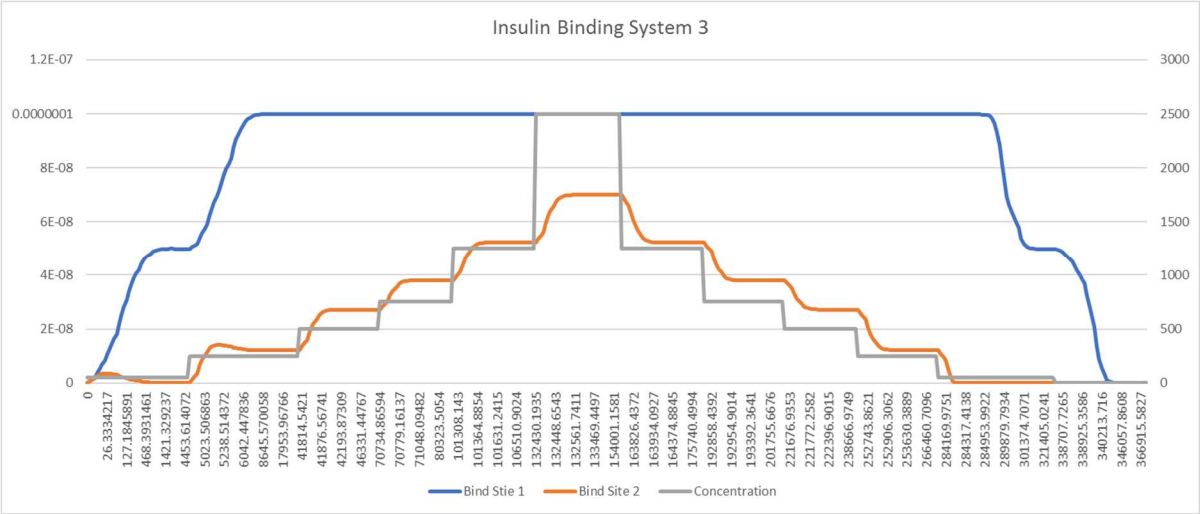

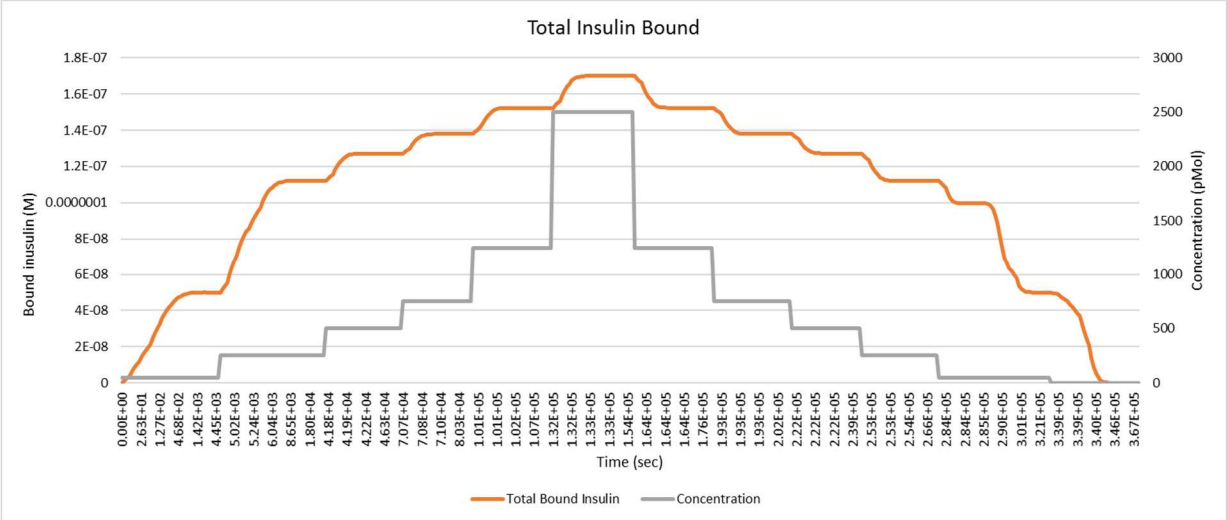

Figure 13**:** The above figures are the concentration fluctuation and the binding affects as seen with settings 3 of the half factorial DOE. The specific settings of the model are shown above. Note that for binding site 1, there is a sudden change in binding, but then

the signal quickly deteriorates which may be to the low antibody concentration, as well as the low dissociation constant. The total binding curve (addition of site 1 and 2) resembles a much-improved fluctuation.

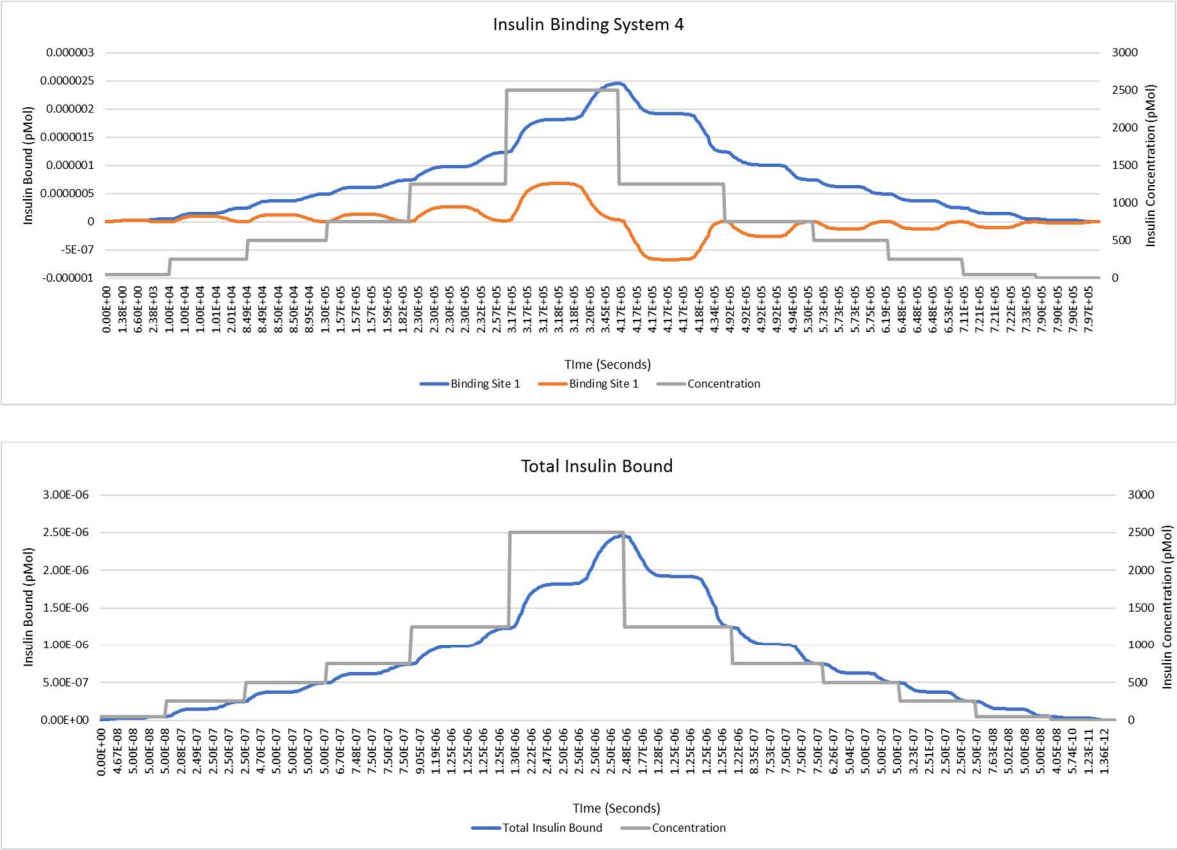

Figure 14**:** The above figures are the concentration fluctuation and the binding affects as seen with settings 4 of the half factorial DOE. The specific settings of the model are shown above. Note that for binding site 1, there shows a nice trend with the increase of concentration. Although the second binding site is much noisier, and does not correlate well on the decreasing concentration. This negative may appear due to the nature of solving the differential equation as a relative negative when compared to the initial value point.

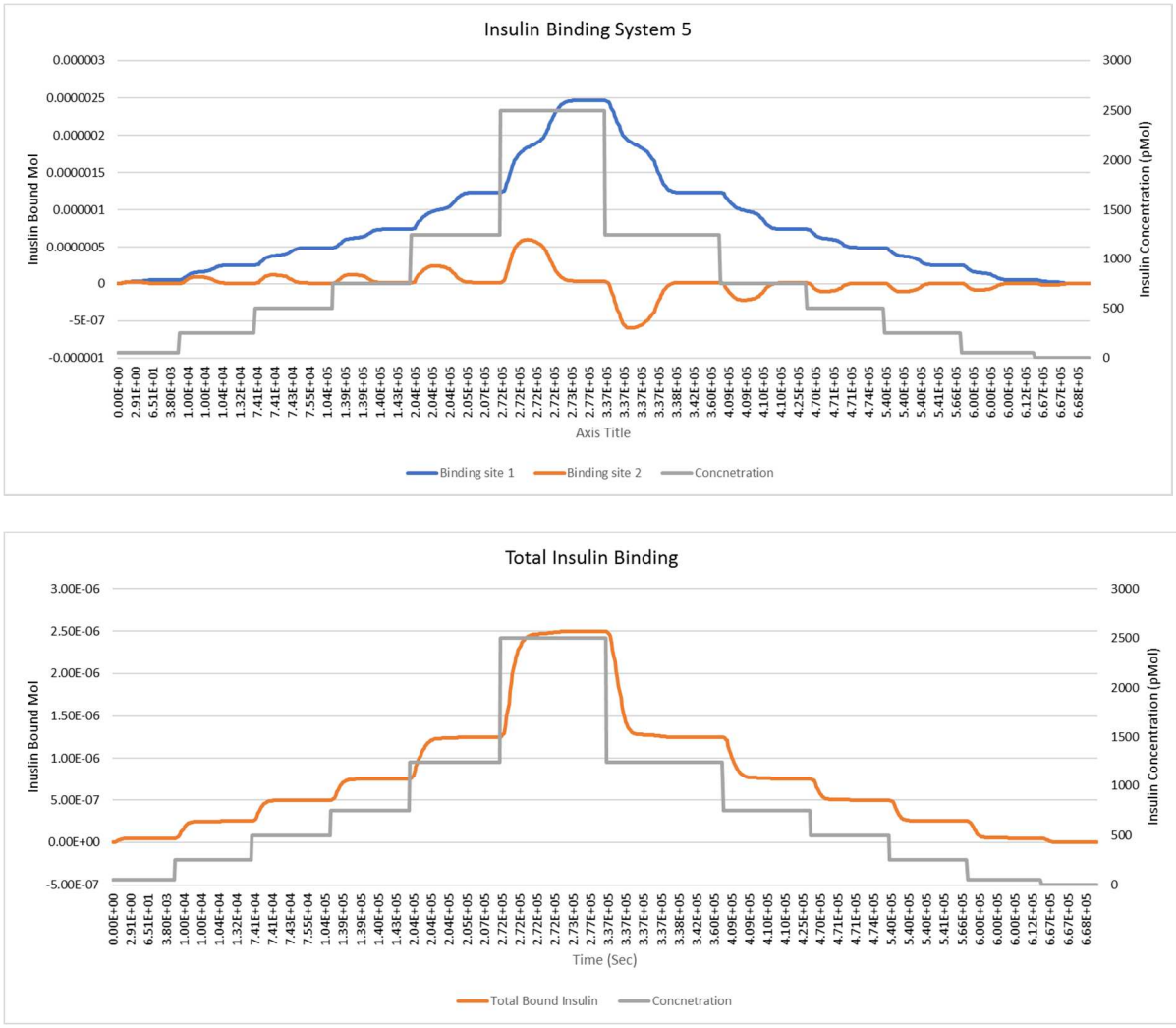

Figure 15**:** The above figures are the concentration fluctuation and the binding affects as seen with settings 5 of the half factorial DOE. The specific settings of the model are shown above. The net binding site has a great trend when compared to other system parameters. Although, like system 4, there is an issue with negative values appearing. Again, this may be due to the simplification of the model, or the need for more specific boundary conditions.

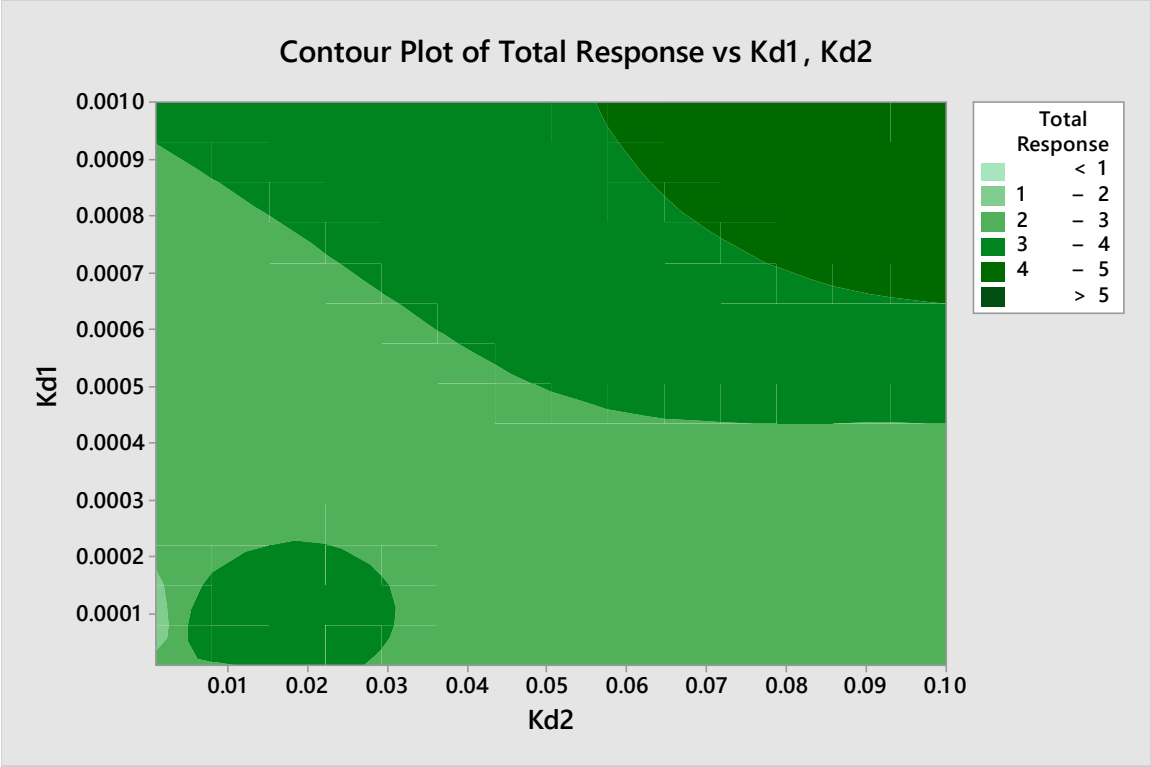

Figure 16**:** The figure above is contour plot showing the different dissociation constants for both binding sites derived from the model. The z-axis is the goodness of fit to the insulin concentration increases. 5 is the best fit, and 1 is the lowest. The contour plot shows that having a higher Kd for both lead to a stronger fit for the concentration. The figure above shows that the ideal Kd for fitting both the increase in insulin and decrease is when both dissociation constants are higher. This would make sense due to the relationship between the half-life of a bond and the dissociation constant.

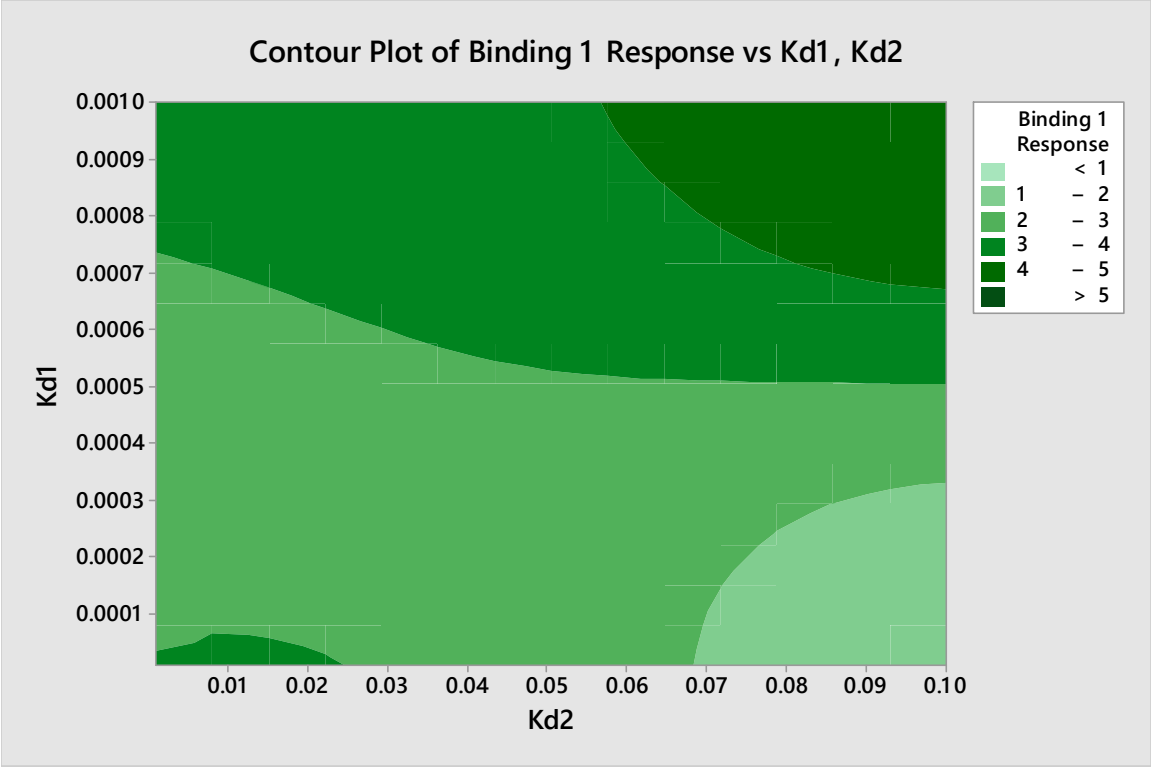

Figure 17**:** The figure above is contour plot showing the different dissociation constants for both binding sites derived from the model. The z-axis is binding response for the first site. The contour plot shows that having a higher Kd for both lead to a stronger fit for the concentration. In addition, the bottom left of the plot also has an area of high affinity binding.

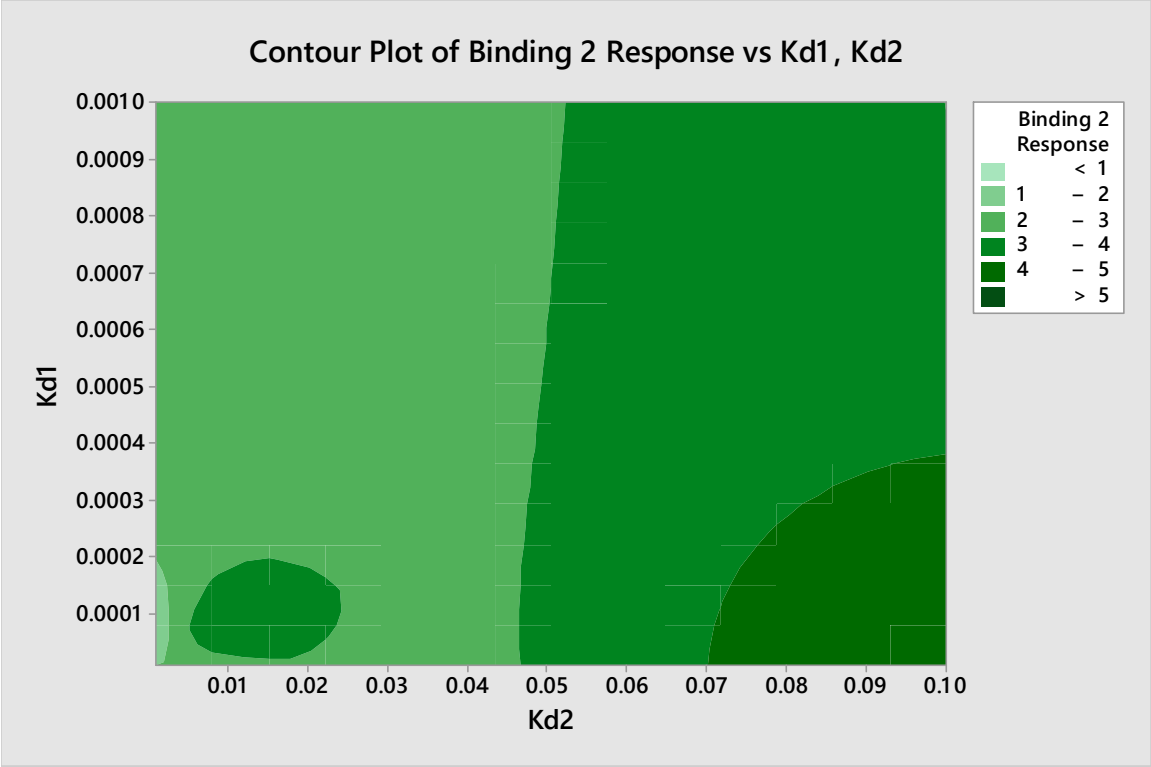

Figure 18**:** The figure above is contour plot showing the different dissociation constants for both binding sites derived from the model. The z-axis is binding response for the first site. The contour plot shows that having a higher Kd for Kd 2 and a lower for Kd1 lead to a stronger fit for the concentration. In addition, the bottom left of the plot also has an area of high affinity binding.

The two figures above represent contour plots relating the dissociation constants for both the binding sites to the goodness of fit of the concentration. These were obtained through the half factorial DOE ran altering the antibody concentration, as well as the two dissociation coefficients.

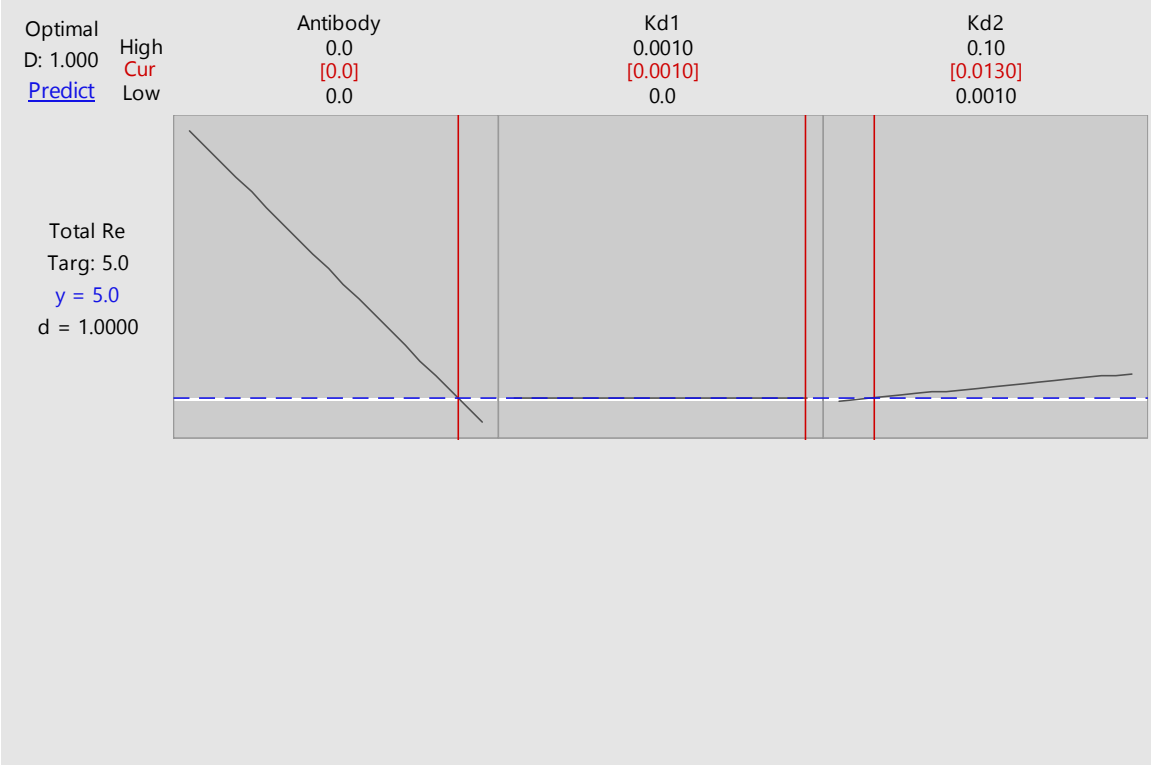

Figure 19**:** Optimization plot for the three input parameters which where antibody, and the two dissociation affinities. The output measurements where to optimize the goodness of fit on a scale of 1-5, with respect to the input insulin concentration.

Variable	Setting
Antibody []	9.178E-06
Kd1	9.927E-04
Kd2	0.0129943

Response	Fit	SE Fit	95% CI	95% PI
Total Response	5.000	*	(*, *)	(*, *)

The figure above is an optimization of the response fit based on three input parameters. These were the two dissociation constants, as well as the concentration of antibody. Using these three aspects the optimization function found the ideal values to be: 9.17uM of IgG antibody that had the Kd values of .01299 for the low affinity site (binding site 2) and 9.9e-4 for the high affinity site (binding site 1). The challenge is the half-life of such a low affinity constant. The fist binding site which has the dissociation constant of 9.92e-4 relates to 770 seconds (12 minutes) for half the antigen to release. The 12-minute half-life can make real time detection very challenging. The attempt to overcome this, another optimizing step was performed based maximizing the dissociation constants. The following figures are the binding curves for site 1, and site two based on the optimization function in minitab.

Assume: The IgG has the dimensions (10 x 2 x7 nm), and a 2mm diameter gold disk electrode, and close packaging .74 can be achieved.

SAelec = Pi*r^2 = 1mm^2*3.14 = 3.14mm^2

SAIgG = (1 nm)*(5 nm) = 1.5708x10-17 m^2

Max Coverage = (.74)*(.0000314 m^2/1.5708x10-17 m^2) = 1.4792462e+13 molecules on the surface. This is equivalent to 2.455e-11M which is much less then what is needed. To bind the required amount of insulin (9.17uM or 5.523e18 molecules) then either the surface area must increase by 4 orders of magnitude, or the packaging must be improved. The needed surface area would be:

(.74)*(X /1.5708x10-17 m^2) = 5.523e18 → X = 117.17 m^2 .

To achieve such a surface area the use of mesoporous carbon, or carbon nanotubes need to be employed. This has been demonstrated by Brittany Cardinal in LaBelle's lab as well as many other fields of research pushing the development of new surface chemistry. Including minimization of half-life:

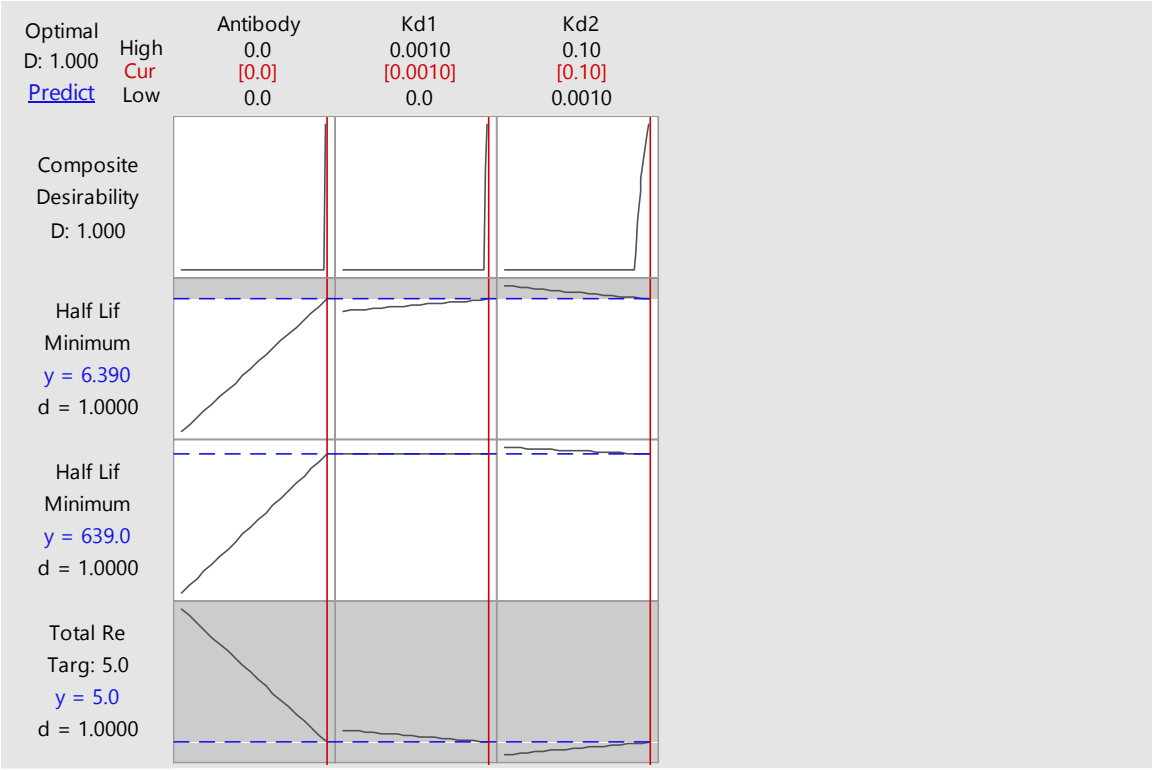

Figure 20**:** Multiple Response Prediction for the model. Showing that the optimal set up has a high antibody concentration, as well as high Kd's for both sites.

Variable	Setting
Antibody []	0.00001
Kd1	0.001
Kd2	0.1

		SE Fit	95% CI	95% PI
Response	Fit			
Half Life Site 2 (Sec)	6.390	*	(*, *)	(*, *)
Half Life Site 1 (sec)	639.0	*	(*, *)	(*, *)
Total Response	5.000	*	(*, *)	(*, *)

The optimization function used above was done to include the addition of half binding for the two sites. The outcome for each was an antibody concentration of 10uM, and the two dissociation constants of .001, and .1 M. The challenge is the time constant which would be approximately 10.65 minutes. Depending on the use case of the patient this may or may not be acceptable for therapy. This then must be translated to the surface of the electrode. As incubating 10uM of antibody will not correlate to that concentration due to steric hindrance, loss in rinsing, and close packaging factors. To achieve this amount of concentration on the surface of the electrode leveraging 16-MHDA interaction can be calculated in the following means:

Assume: The IgG has the dimensions (10 x 2 x7 nm), and a 2mm diameter gold disk electrode, and close packaging .74 can be achieved.

SAelec = Pi*r^2 = 1mm^2*3.14 = 3.14mm^2

SAIgG = (1 nm)*(5 nm) = 1.5708x10-17 m^2

Max Coverage = (.74)*(.0000314 m^2/1.5708x10-17 m^2) = 1.4792462e+13 molecules on the surface. This is equivalent to 2.455e-11M which is much less then what is needed. To bind the required amount of insulin (10uM or 6.023e17 molecules) then either the surface

area must increase by 4 orders of magnitude, or the packaging must be improved. The needed surface area would be:

$$(.74)*(X\ /1.5708x10\text{-}17\ m^2) = 6.023e17 \rightarrow X = 12.78\ m^2\ .$$

To achieve such a surface area the use of mesoporous carbon, or carbon nanotubes need to be employed.

Kinetic Model with Optimized Parameter:

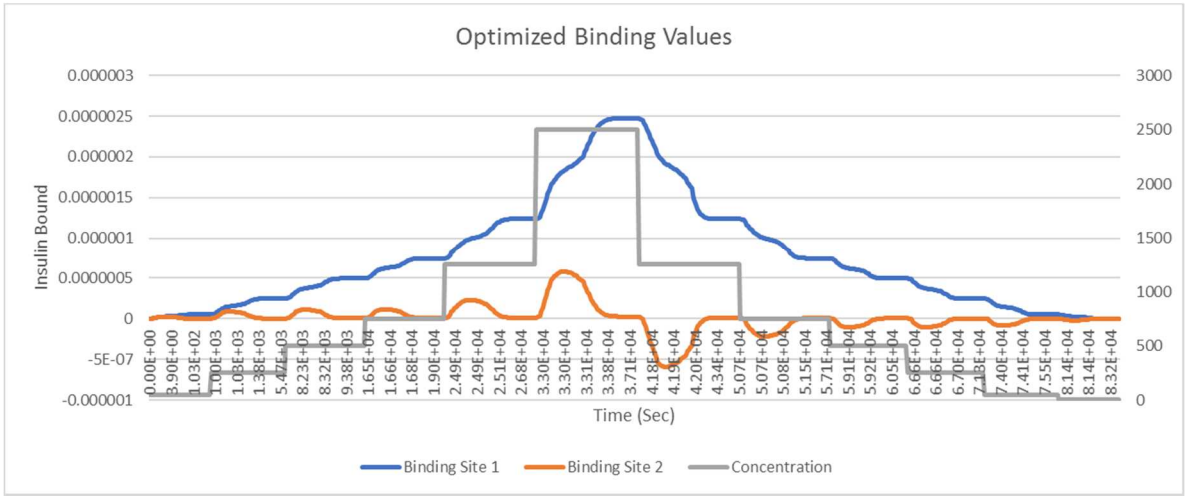

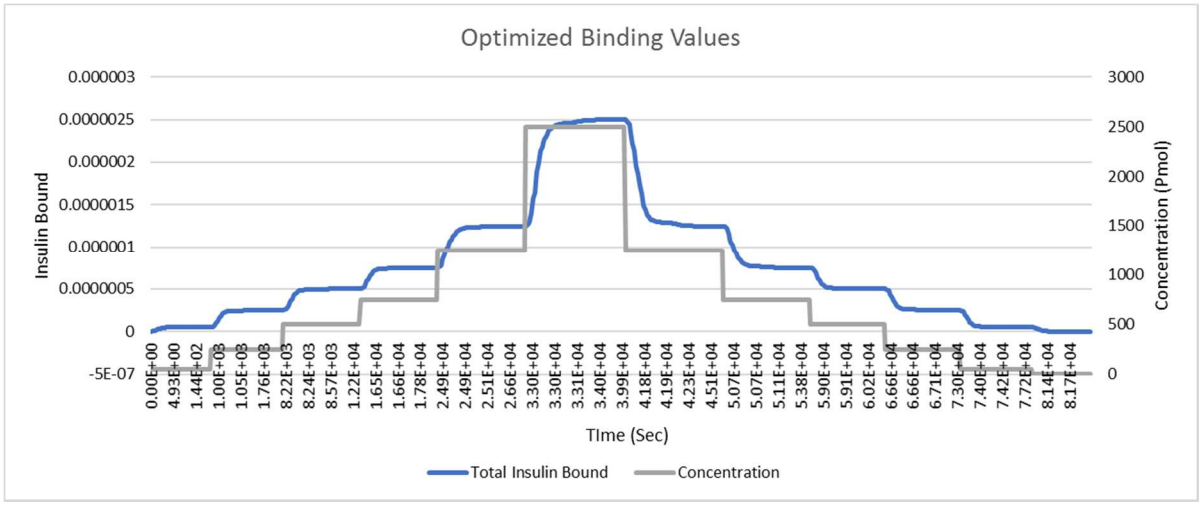

Figure 21**:** Once the optimization function was performed in mintab, the new parameters where input into the matlab model. These results show a nice relationship between the input concentration, as with binding.

The models above where done on the matlab code given by Dr. Capaln, to help validate the writing of another general differential equation solver was done. The second code is written below, which used 4 differential equations, one for the insulin free, unbound antibody, and the 2 binding sites. In this case, we only test the optimal values derived off the optimization function in minitab.

```
function rre_AB
tspan = [0 4000]; yzero = [50e-9; 1e-7; 0; 0];
k1 = 3e5; k2 = 1e-5; k3 = 3e5; k4 = 1e-2;
[t,y] = ode15s(@AB_rre,tspan,yzero)
plot (t, y)
function ypI = AB_rre(t,y)
ypI = zeros(4,1);
ypI(1) = -k2*y(3) - k1*y(1)*y(2) + k4*y(4) - k3*y(1)*y(3); %Blue Curve (Free insulin)
ypI(2) = k2*y(3) - k1*y(1)*y(2);%Orange Curve (Unbound antibody
ypI(3) = k1*y(1)*y(2) - (k2)*y(3) + k4*y(4) - k3*y(1)*y(3); %Yellow Curve (Antibody
with 1 bound)
ypI(4) = -k4*y(4) + k3*y(1)*y(3); %Purple Curve (antibody with 2 bonds)
end
end
```

CHAPTER 4

BACKGROUND OF EIS AND OPTIMAL FREQUENCY FOR INSULIN

Electrochemical impedance spectroscopy is an electrochemical method that interrogates a system utilizing an alternating current signal. The signal is swept through a series of frequencies that range from 1Hz up to 100KHz. The measured output of the system is phase and impedance which can be related to the input factors of the system. EIS offers various advantages for biosensing, including improved sensitivity, label-free detection and speed (< 90 seconds). It measures the resistance and capacitance of an electrochemical system with variable AC signal. The AC signal consists of a varying potential and a wide range AC frequency sweep. When varying AC signals are applied to the sample of interest, a current response is generated. The current response is measured over the range of frequencies encompassed by the sweep and is then used to calculate the real, imaginary, phase angle, and complex impedance. Mathematically, the complex impedance is defined by the equation below:

$$(j\omega) = \frac{U(j\omega)}{I(j\omega)} = Z_r(\omega) + jZ_i(\omega) \quad \text{Eq. 17}$$

Where, is the complex impedance, the angular frequency (which is equivalent to where is the input frequency), the applied potential, the current response, the real impedance, and the imaginary impedance. After investigating the correlation between the complex impedance and target concentration, the concept of optimal frequency is applied. The optimal frequency of a biomarker is the AC frequency at which the resulting impedance best represents the interaction between the biomarker and its molecular recognition element (MREs). The optimal frequency is determined by optimizing the responsivity and R-square values (RSQ). It offers an orthogonal means for target detection in addition

to the specific interaction between target and their MREs. By determining the optimal frequencies of the biomarkers of interest, it is proposed that each biomarker can be detected at its optimal frequency simultaneously on a single sensor platform, envisioning the possibility of a multi-marker detection platform technology. In addition to this various other parameter can be measured. These include capacitance, resistance, conductance, admittance, and modulus. These different parameters all give distinct information about the entire system. This can be useful for characterizing materials such as polymers, co-polymers, and such. Furthermore, electron kinetics can be interrogated using EIS, which is seen generally through the Warburg style plot (Tacrolimus not yet submitted).

EIS has begun to get more attention as well as various derivatives of the method such as electrochemical capacitance spectroscopy being developed and implanted by James Davis and others. EIS depends on the theory that each biomarker as a specific and unique binding frequency. This has been developed for both single marker detection and multimarker methods ([88], [92], [93], [100]–[107]).

Optimal Frequency (The following section is derived from Lin. Et. Al. (submitted))

The optimal frequency has been used by various researchers to quantify the concentration of biomolecular interacts that occur on the surface of the electrode. Dr. Lin reported various inputs that may affect the frequency at which this signal peaks ([92], [101], [108]–[111]). The general cut off frequency has been modeled as the following:

$$f_c = \frac{1}{\mathrm{RC}2\pi} \quad \text{Eq. 18}$$

where R is resistance and C the capacitance. The equation can be used to explain the changes of optimal frequencies discovered in the biomarker using the inputs of zeta potential, molecular weight, and conductivity which are unique to any one interaction. These were extensively studied by Lin et al, using the conjugation of nanoparticles to electrode surface and a series of design of experiments to produce a calibration curve relating the zeta, conductivity, and mass of a system to the predicted optimal frequency. The values of zeta potential and conductivity of nanoparticles and biomarker analytes are measured in a free-flowing model, which was different from the immobilized model used herein. For the case of insulin, all these values will be approximated through literature and other studies.

Zeta potential is generally defined as the electrostatic potential at the interfacial double layer of the between the particles and the surrounding mediums ([112]). Zeta potential can also a molecule's surface charge, although this is an average of an entire system. This surface charge then can affect the expected optimal frequency and is used in the analysis of insulin. Nevertheless, as shown in by Lin et al. zeta potential can significantly affect the optimal frequency. In general, higher negative charge on the surface of particles might restrict the flow of electron and thus increase the charge transfer resistance, therefore corresponds to the lower optimal frequency recorded ([108], [113], [114]) according to Equation 18.

An increase in the molecular weight of a molecule results in a decrease in the optimal frequency as observed by Lin et al. The increase in molecular weight may cause steric hindrance and close packing limitations near the electrode surface, as the electron flows through the antibody-antigen or nanoparticle-antibody-antigen complexes are obstructed.

A larger molecular weight can be attributed to the size and/or density of the molecule. Assuming both the antigen-antibody are spheres with a hydrodynamic radius of r, their resistance and capacitance can be modeled as:

$$R = \rho\frac{2\pi r}{\pi r^2} = \rho\frac{2}{r} \quad \text{Eq. 19}$$

$$C = \frac{2\pi\varepsilon_0\varepsilon_r}{1+\frac{d}{r}} \quad \text{Eq. 20 Chaki et al.}$$

where ρ is the resistivity, ε the dielectric constant of the sphere, ε_r the permittivity of the medium, and d the distance between the antibody-antigen complex and the surface of the electrode. According to equation 19 and 20, when the molecular weight changes, the change in size and/or density can be reflected in r and d, resulting in a change in the resistance and capacitance.

However, changing the molecular weight can also affect the ρ and ε of the antibody complex due the alternating current applied in the EIS and a change in the close packing factor ([115]–[117]), affecting the resistance and capacitance of the antibody complex. Since r and d are in the denominator and ρ and ε the numerator, altering the molecular weight will have trade-off effects depending on the magnitudes of these factors. Judging from Equation 18 an increase in the molecular weight suggested an overall increase in the resistance and the capacitance, meaning that the growths in ρ and ε are more dominant than that of r and d. In other words, an increase in the molecular weight would affect the electron flows inside the antibody complex, increase both its resistance and the capacitance, and thus lower the cutoff frequency and consequently the optimal frequency according to Equation 18. Increasing the molecular weight can also lead to a larger

surface area for charge accumulation, affecting the zeta potential around the particles and consequently the antibody complex.

Conductivity is also a factor that significantly affects the optimal frequency. The conductivity measures how the electrons flow through a material and is the reciprocal of resistivity. Using the similar boundary conditions above, the conductivity of the antigen and the nanoparticles can also affect the conductivity of the overall complex. Subsequently, the flow of electrons through the complex to the electrode is affected. Therefore, conductivity of the overall system can affect the resistance in the equivalent circuit, consequently affecting the optimal frequency.

Significant interaction between the conductivity and zeta was also found to affect the optimal frequency. Since zeta potential is an estimation of the surface charge between the molecule and the surrounding medium, the repulsion among molecules can affect the electron flow through the antibody complex as well. Therefore, the interaction between conductivity and zeta can affect the resistance and capacitance of the antibody complex, and consequently the optimal frequency. The conductivity of the antibody complex can be modeled as:

$\sigma = \sigma_0 \, e^{(-E\_a/RT)}$ Eq. 21 obtained from Brust et al.

$E_a = \frac{e^2}{8\pi\varepsilon_0\varepsilon_r}\left(\frac{1}{r} - \frac{1}{r+d}\right)$ Eq. 22 from Brust et al.

where σ is the conductivity constant, E the activation energy, R the universal gas constant, T the temperature, and e the charge of an electron. As described above, the change in the molecular weight may also affect ρ, ε, r, and d, as well as varies other parameters. Using these various inputs and the transfer function derived from Lin et al, we could predict where the peak frequency should be based on the mass, conductivity

and zeta of insulin found in literature. The next goal is to predict what the change in impedance may be due to insulin binding. To simplify this model, we are assuming the system acts as a perfect capacitor, and has no electron transfer during the interaction of inulin and the antibody. The following chart was reprinted with permission of Lin et al. which shows the initial DOE built to predict optimal frequency, as well as the transfer function derived from the experiments:

$$F_o = 274.36 + 8.03E^{-3}\sigma + 9.59\zeta - 2.91E^{-5}m - 1.34E^{-3}\sigma\zeta + 2.18E^{-8}\sigma m - 6.89E^{-7}\zeta m \quad \text{Eq. 23}$$

where F_o is the optimal frequency, σ the conductivity in, ζ the zeta potential, and m the molecular weight. The following chart presents the approximate values for these of insulin based on others published work. Immediately there are challenges found in attempting to apply this model to insulin. This begins with mass, insulin alone as a mass ranging around 5733.55 g./mol (Pubchem.gov) but as the concentration increase, insulin may aggregate together which will increase the overall mass of the system. Insulin has been thought to aggregate at lower concentrations levels, which may affect the predicted mass of the protein. For this model, we will assume monomer insulin molecules only. The second parameter of interest is conductivity. This also has been shown to be dependent on the concentration of insulin available in solution ([118]). Omathanu Pillai et al showed that as insulin concentration increases, the conductivity of the solution also does. This may be in part related to the aggregation challenges of the protein or may be due to steric effects of charge. Although the conductivity of the insulin molecule will still be constant, the system interaction effects seem to impact the mixtures conductivity. First starting with the monomer, the mass is 57733.55 daltons. To get the conductance, we

leveraged the relationship between impedance which is the inverse of the conductance. This led to another interesting point, which is that Dr. Lin used DC based conductance, whereas here we use an AC based conductance. The difference would be thought to be small due to the 5 mV bias applied. The concept that conductance may be frequency dependent calls into question the work done previously, as well as if there are superior methods. Nonetheless, the calculated conductance was 2.61 uS. The zeta potential was estimated to be about -15mV, this value comes from two sources. First is literature which cites a range of that, in addition previous IgG antibodies character for lactoferrin also showed a Zeta of -15mV. The same analysis was done for the oligomer, but with 1 main difference. This is that there is currently no data on how many insulin molecules are oligomerized with each other. To overcome this, the assumption that there is normal distribution of molecules bound ranging from 10, up to 10000. Using this bookending, the mean frequency was then chosen as the most likely value based on the distribution. Below table 2 summarized the results from the analysis.

MONOMER (Group 1)
Mass: 5733.55
Conductivity: Assume to be 1/R and measure at peak response: ~2.61 uS
Zeta Potential: -15mV
Optimal Frequency: 130.81 Hz

- Note: 130.81 Hz is nearly on the dot for the measured peak with blank at 146 Hz, and is off by about 3 points for the without peak at 69.75 Hz

OLIGOMER (Group 2)
Mass Range: 57335.5 – 5735500.00
Conductivity: Assume to be 1/R and measure at peak response: ~18.51 uS
Zeta Potential: -15mV
Optimal Frequency: 380.24 – 2623.18 Hz → Average the range ~1500 Hz

- Note: 1500 Hz is about 3 data points off our measured 966 Hz with blank, and 2 data point off without blank measured at 1172 Hz

Table 2: The above image shows the calculated optimal frequency based upon the various size distributions, as well as the change in conductance.

This helps depict what may have caused the two peaks to occur. This also may be an enabled technology to predict the amount of oligomerization of insulin manufactures using the location of the peak. There are a few key assumptions used in the model above which do need to validate in lab through an orthogonal method. First is the conductivity which is calculated through the impedance measurement's done using the EIS system described. In addition, the fact that we utilized an transfer function based on DC using AC values and still predicted correctly may suggest that the type of analysis to measure the conductivity may not matter. Or that the 5mV bias is not great enough to impact the conductivity measurement compared to that of a DC method. The next important assumption in the model is that the zeta potential does not change with oligomerization. This is not entirely true since the amount of available surface areas to the surrounding medium may impact that double layer capacitance of that system and in turn the zeta. The last major assumption is the distribution of mass. The assumed state is Gaussian, as well as the limits of 10 self-bound up to 10000. This assumption may be very incorrect, as the range may span to millions of molecules or even lower than 10. Yet, the ability to use the transfer function to help predict yet another molecule adds more validity to that derived equation.

References

[1] L. C. Clark and C. Lyons, "Electrode systems for continuous monitoring in cardiovascular surgery," *Annals of the New York Academy of sciences*, vol. 102, no. 1, pp. 29–45, 1962.

[2] D. M. Angaran, D. F. Smith, and M. L. Birnbaum, "Use of Clinitest urine test for indirect estimation of blood glucose levels in the critically ill," *Am J Hosp Pharm*, vol. 37, no. 7, pp. 950–956, Jul. 1980.

[3] D. Rodbard, "Continuous Glucose Monitoring: A Review of Successes, Challenges, and Opportunities," *Diabetes Technol Ther*, vol. 18, no. Suppl 2, pp. S2-3-S2-13, Feb. 2016.

[4] G. G. Guilbault and G. J. Lubrano, "An enzyme electrode for the amperometric determination of glucose," *Analytica chimica acta*, vol. 64, no. 3, pp. 439–455, 1973.

[5] E.-H. Yoo and S.-Y. Lee, "Glucose biosensors: an overview of use in clinical practice," *Sensors*, vol. 10, no. 5, pp. 4558–4576, 2010.

[6] J. Wang, "Electrochemical glucose biosensors," *Chemical reviews*, vol. 108, no. 2, pp. 814–825, 2008.

[7] M. K. Weibel and H. J. Bright, "The glucose oxidase mechanism interpretation of the pH dependence," *Journal of Biological Chemistry*, vol. 246, no. 9, pp. 2734–2744, 1971.

[8] S. A. Emr and A. M. Yacynych, "Use of polymer films in amperometric biosensors," *Electroanalysis*, vol. 7, no. 10, pp. 913–923, 1995.

[9] C. Malitesta, F. Palmisano, L. Torsi, and P. G. Zambonin, "Glucose fast-response amperometric sensor based on glucose oxidase immobilized in an electropolymerized poly (o-phenylenediamine) film," *Analytical Chemistry*, vol. 62, no. 24, pp. 2735–2740, 1990.

[10] F. Palmisano, D. Centonze, A. Guerrieri, and P. G. Zambonin, "An interference-free biosensor based on glucose oxidase electrochemically immobilized in a non-conducting poly (pyrrole) film for continuous subcutaneous monitoring of glucose through microdialysis sampling," *Biosensors and Bioelectronics*, vol. 8, no. 9–10, pp. 393–399, 1993.

[11] R. Sternberg, D. S. Bindra, G. S. Wilson, and D. R. Thevenot, "Covalent enzyme coupling on cellulose acetate membranes for glucose sensor development," *Analytical Chemistry*, vol. 60, no. 24, pp. 2781–2786, 1988.

[12] M. G. Sevag, J. Henry, and R. A. Richardson, “Studies on the Action of Sulfonamides on the Respiration and Growth of Bacteria: B. Factors Influencing the Correlation of the Inhibition of Respiration with the Inhibition of Growth of Escherichia coli, Pneumococcus, Type 1, and Staphylococcus aureus I. The Interference of the Evolution of Hydrogen with the Measurement of the Inhibition of Oxygen Consumption in Escherichia coli,” *Journal of bacteriology*, vol. 49, no. 2, p. 129, 1945.

[13] M. Stephenson, “Some aspects of hydrogen transfer,” *Antonie van Leeuwenhoek*, vol. 12, no. 1–4, pp. 33–48, 1947.

[14] Y. Degani and A. Heller, “Direct electrical communication between chemically modified enzymes and metal electrodes. 2. Methods for bonding electron-transfer relays to glucose oxidase and D-amino-acid oxidase,” *Journal of the American Chemical Society*, vol. 110, no. 8, pp. 2615–2620, 1988.

[15] Y. Degani and A. Heller, “Electrical communication between redox centers of glucose oxidase and electrodes via electrostatically and covalently bound redox polymers,” *Journal of the American Chemical Society*, vol. 111, no. 6, pp. 2357–2358, 1989.

[16] A. Heller, “Concepts of electrically connecting redox enzymes to metal electrodes.,” *American biotechnology laboratory*, vol. 8, no. 8, p. 14, 1990.

[17] M. V. Pishko, I. Katakis, S.-E. Lindquist, A. Heller, and Y. Degani, “Electrical communication between graphite electrodes and glucose oxidase/redox polymer complexes,” *Molecular Crystals and Liquid Crystals*, vol. 190, no. 1, pp. 221–249, 1990.

[18] A. Heller, “Electrical wiring of redox enzymes,” *Accounts of Chemical Research*, vol. 23, no. 5, pp. 128–134, 1990.

[19] M. V. Pishko, I. Katakis, S.-E. Lindquist, L. Ye, B. A. Gregg, and A. Heller, “Direct electron exchange between graphite electrodes and an adsorbed complex of glucose oxidase and an osmium-containing redox polymer,” *Angew. Chem., Int. Ed*, vol. 102, no. 1, pp. 109–11, 1990.

[20] B. A. Gregg and A. Heller, “Cross-linked redox gels containing glucose oxidase for amperometric biosensor applications,” *Analytical Chemistry*, vol. 62, no. 3, pp. 258–263, 1990.

[21] R. Maidan and A. Heller, “Elimination of electrooxidizable interferants in glucose electrodes,” *Journal of the American Chemical Society*, vol. 113, no. 23, pp. 9003–9004, 1991.

[22] B. A. Gregg and A. Heller, “Redox polymer films containing enzymes. 2. Glucose oxidase containing enzyme electrodes,” *The Journal of Physical Chemistry*, vol. 95, no. 15, pp. 5976–5980, 1991.

[23] C. M. Wang, A. Heller, and H. Gerischer, “Palladium catalysis of O2 reduction by electrons accumulated on TiO2 particles during photoassisted oxidation of organic compounds,” *Journal of the American Chemical Society*, vol. 114, no. 13, pp. 5230–5234, 1992.

[24] T. J. Ohara, R. Rajagopalan, and A. Heller, “Glucose electrodes based on cross-linked bis (2, 2’-bipyridine) chloroosmium (+/2+) complexed poly (1-vinylimidazole) films,” *Analytical Chemistry*, vol. 65, no. 23, pp. 3512–3517, 1993.

[25] T. J. Ohara, R. Rajagopalan, and A. Heller, “‘ Wired’ Enzyme Electrodes for Amperometric Determination of Glucose or Lactate in the Presence of Interfering Substances,” *Analytical Chemistry*, vol. 66, no. 15, pp. 2451–2457, 1994.

[26] W. Kerner, S. E. Lindquist, M. V. Pishko, and A. Heller, “Amperometric glucose sensor containing glucose oxidase cross-linked in redox gels,” *In Vivo Chemical Sensors: Recent Developments*, 1993.

[27] A. Aoki and A. Heller, “Electron diffusion coefficients in hydrogels formed of cross-linked redox polymers,” *The Journal of Physical Chemistry*, vol. 97, no. 42, pp. 11014–11019, 1993.

[28] L. Ye *et al.*, “High current density" wired" quinoprotein glucose dehydrogenase electrode,” *Analytical Chemistry*, vol. 65, no. 3, pp. 238–241, 1993.

[29] I. Katakis, L. Ye, G. Kenausis, and A. Heller, “DESIGN OF REDOX POLYELECTROLYTE WIRES FOR GLUCOSE ELECTRODES,” in *ABSTRACTS OF PAPERS OF THE AMERICAN CHEMICAL SOCIETY*, 1994, vol. 208, pp. 321-PMSE.

[30] B. Linke, W. Kerner, M. Kiwit, M. Pishko, and A. Heller, “Amperometric biosensor for in vivo glucose sensing based on glucose oxidase immobilized in a redox hydrogel,” *Biosensors and Bioelectronics*, vol. 9, no. 2, pp. 151–158, 1994.

[31] E. Csoeregi *et al.*, “Design, characterization, and one-point in vivo calibration of a subcutaneously implanted glucose electrode,” *Analytical Chemistry*, vol. 66, no. 19, pp. 3131–3138, 1994.

[32] I. Katakis, L. Ye, and A. Heller, “Electrostatic Control of the Electron-Transfer Enabling Binding of Recombinant Glucose Oxidase and Redox Polyelectrolytes,” *Journal of the American Chemical Society*, vol. 116, no. 8, pp. 3617–3618, 1994.

[33] C. P. Quinn *et al.*, “Kinetics of glucose delivery to subcutaneous tissue in rats measured with 0.3-mm amperometric microsensors,” *American Journal of Physiology-Endocrinology And Metabolism*, vol. 269, no. 1, pp. E155–E161, 1995.

[34] C. P. Quinn, C. P. Pathak, A. Heller, and J. A. Hubbell, “Photo-crosslinked copolymers of 2-hydroxyethyl methacrylate, poly (ethylene glycol) tetra-acrylate and ethylene dimethacrylate for improving biocompatibility of biosensors,” *Biomaterials*, vol. 16, no. 5, pp. 389–396, 1995.

[35] L. Gorton, “On-Line Glucose Monitoring by Using Microdialysis Sampling and Amperometric Detection Based on’Wired’Glucose Oxidase in Carbon Paste,” *Mikrochim. Acta*, vol. 121, pp. 31–40, 1995.

[36] T. de Lumley-Woodyear, P. Rocca, J. Lindsay, Y. Dror, A. Freeman, and A. Heller, “Polyacrylamide-based redox polymer for connecting redox centers of enzymes to electrodes,” *Analytical chemistry*, vol. 67, no. 8, pp. 1332–1338, 1995.

[37] E. Csoeregi, D. W. Schmidtke, and A. Heller, “Design and optimization of a selective subcutaneously implantable glucose electrode based on" wired" glucose oxidase,” *Analytical Chemistry*, vol. 67, no. 7, pp. 1240–1244, 1995.

[38] I. Willner *et al.*, “Electrical wiring of glucose oxidase by reconstitution of FAD-modified monolayers assembled onto Au-electrodes,” *Journal of the American Chemical Society*, vol. 118, no. 42, pp. 10321–10322, 1996.

[39] A. R. Vijayakumar, E. Csöregi, A. Heller, and L. Gorton, “Alcohol biosensors based on coupled oxidase-peroxidase systems,” *Analytica Chimica Acta*, vol. 327, no. 3, pp. 223–234, 1996.

[40] T. de Lumley-Woodyear, C. N. Campbell, and A. Heller, “Direct enzyme-amplified electrical recognition of a 30-base model oligonucleotide,” *Journal of the American Chemical Society*, vol. 118, no. 23, pp. 5504–5505, 1996.

[41] R. Rajagopalan, A. Aoki, and A. Heller, “Effect of quaternization of the glucose oxidase ‘wiring’ redox polymer on the maximum current densities of glucose electrodes,” *The Journal of Physical Chemistry*, vol. 100, no. 9, pp. 3719–3727, 1996.

[42] C. Taylor, G. Kenausis, I. Katakis, and A. Heller, “‘Wiring’ of glucose oxidase within a hydrogel made with polyvinyl imidazole complexed with [(Os-4, 4′-dimethoxy-2, 2′-bipyridine) Cl]+/2+ 1,” *Journal of Electroanalytical Chemistry*, vol. 396, no. 1–2, pp. 511–515, 1995.

[43] R. Rajagopalan and A. Heller, *Electrical ‘wiring’of glucose oxidase in electron conducting hydrogels*. Blackwell Science Ltd, Cambridge, MA, 1997.

[44] G. Kenausis, C. Taylor, I. Katakis, and A. Heller, "'Wiring'of Glucose Oxidase and Lactate Oxidase Within a Hydrogel Made with Poly (vinyl pyridine) complexed with [Os (4, 4′-dimethoxy-2, 2′-bipyridine) 2Cl]+/2+," *Journal of the Chemical Society, Faraday Transactions*, vol. 92, no. 20, pp. 4131–4136, 1996.

[45] C. A. Quinn, R. E. Connor, and A. Heller, "Biocompatible, glucose-permeable hydrogel for in situ coating of implantable biosensors," *Biomaterials*, vol. 18, no. 24, pp. 1665–1670, 1997.

[46] J. G. Wagner, D. W. Schmidtke, C. P. Quinn, T. F. Fleming, B. Bernacky, and A. Heller, "Continuous amperometric monitoring of glucose in a brittle diabetic chimpanzee with a miniature subcutaneous electrode," *Proceedings of the National Academy of Sciences*, vol. 95, no. 11, pp. 6379–6382, 1998.

[47] T. Terse-Thakoor, K. Komori, P. Ramnani, I. Lee, and A. Mulchandani, "Electrochemically functionalized seamless three-dimensional graphene-carbon nanotube hybrid for direct electron transfer of glucose oxidase and bioelectrocatalysis," *Langmuir*, vol. 31, no. 47, pp. 13054–13061, 2015.

[48] Y. Ogawa, S. Yoshino, T. Miyake, and M. Nishizawa, "Surfactant-assisted direct electron transfer between multi-copper oxidases and carbon nanotube-based porous electrodes," *Physical Chemistry Chemical Physics*, vol. 16, no. 26, pp. 13059–13062, 2014.

[49] J. Okuda, J. Wakai, N. Yuhashi, and K. Sode, "Glucose enzyme electrode using cytochrome b562 as an electron mediator," *Biosensors and Bioelectronics*, vol. 18, no. 5–6, pp. 699–704, 2003.

[50] J. Okuda and K. Sode, "PQQ glucose dehydrogenase with novel electron transfer ability," *Biochemical and biophysical research communications*, vol. 314, no. 3, pp. 793–797, 2004.

[51] H. Yoshida, G. Sakai, K. Mori, K. Kojima, S. Kamitori, and K. Sode, "Structural analysis of fungus-derived FAD glucose dehydrogenase," *Scientific reports*, vol. 5, p. 13498, 2015.

[52] I. Lee *et al.*, "The electrochemical behavior of a FAD dependent glucose dehydrogenase with direct electron transfer subunit by immobilization on self-assembled monolayers," *Bioelectrochemistry*, vol. 121, pp. 1–6, 2018.

[53] L. Liu, W. Qi, X. Gao, C. Wang, and G. Wang, "Synergistic effect of metal ion additives on graphitic carbon nitride nanosheet-templated electrodeposition of Cu@ CuO for enzyme-free glucose detection," *Journal of Alloys and Compounds*, vol. 745, pp. 155–163, 2018.

[54] V. Veeramani, R. Madhu, S.-M. Chen, P. Veerakumar, C.-T. Hung, and S.-B. Liu, "Heteroatom-enriched porous carbon/nickel oxide nanocomposites as enzyme-free

highly sensitive sensors for detection of glucose," *Sensors and Actuators B: Chemical*, vol. 221, pp. 1384–1390, 2015.

[55] N. Senthilkumar, K. J. Babu, G. Gnana kumar, A. R. Kim, and D. J. Yoo, "Flexible electrospun PVdF-HFP/Ni/Co membranes for efficient and highly selective enzyme free glucose detection," *Industrial & Engineering Chemistry Research*, vol. 53, no. 25, pp. 10347–10357, 2014.

[56] X. Li *et al.*, "Impedimetric Enzyme-Free Detection of Glucose via a Computation-Designed Molecularly Imprinted Electrochemical Sensor Fabricated on Porous Ni Foam," *Electroanalysis*, vol. 29, no. 5, pp. 1243–1251, 2017.

[57] H. Çiftçi, U. Tamer, M. Ş. Teker, and N. Ö. Pekmez, "An enzyme free potentiometric detection of glucose based on a conducting polymer poly (3-aminophenyl boronic acid-co-3-octylthiophene)," *Electrochimica Acta*, vol. 90, pp. 358–365, 2013.

[58] Y. Hu, X. Niu, H. Zhao, J. Tang, and M. Lan, "Enzyme-free amperometric detection of glucose on platinum-replaced porous copper frameworks," *Electrochimica Acta*, vol. 165, pp. 383–389, 2015.

[59] A. Heller and B. Feldman, "Electrochemistry in diabetes management," *Accounts of chemical research*, vol. 43, no. 7, pp. 963–973, 2010.

[60] B. Feldman, R. Brazg, S. Schwartz, and R. Weinstein, "A continuous glucose sensor based on Wired Enzyme^{TM} technology-Results from a 3-day trial in patients with type 1 diabetes," *Diabetes technology & therapeutics*, vol. 5, no. 5, pp. 769–779, 2003.

[61] O. Barbosa, C. Ortiz, Á. Berenguer-Murcia, R. Torres, R. C. Rodrigues, and R. Fernandez-Lafuente, "Glutaraldehyde in bio-catalysts design: a useful crosslinker and a versatile tool in enzyme immobilization," *Rsc Advances*, vol. 4, no. 4, pp. 1583–1600, 2014.

[62] S. K. Vashist, D. Zheng, K. Al-Rubeaan, J. H. Luong, and F.-S. Sheu, "Technology behind commercial devices for blood glucose monitoring in diabetes management: A review," *Analytica chimica acta*, vol. 703, no. 2, pp. 124–136, 2011.

[63] D. C. Klonoff *et al.*, "The Surveillance Error Grid," *Journal of Diabetes Science and Technology*, vol. 8, no. 4, pp. 658–672, Jul. 2014.

[64] F. Reiterer *et al.*, "Significance and Reliability of MARD for the Accuracy of CGM Systems," *Journal of Diabetes Science and Technology*, vol. 11, no. 1, pp. 59–67, Jan. 2017.

[65] “2016 FDA standard for glucose sensor - Google Search.” [Online]. Available: https://www.google.com/search?q=2016+FDA+standard+for+glucose+sensor&rlz=1C1GGRV_enUS751US751&oq=2016+FDA+standard+for+glucose+sensor&aqs=chrome..69i57.5304j0j7&sourceid=chrome&ie=UTF-8. [Accessed: 08-Apr-2018].

[66] “Self-Monitoring Blood Glucose Test Systems for Over-the-Counter Use - Guidance for Industry and Food and Drug Administration Staff,” p. 43.

[67] B. H. Ginsberg, “Factors affecting blood glucose monitoring: sources of errors in measurement,” *Journal of diabetes science and technology*, vol. 3, no. 4, pp. 903–913, 2009.

[68] R. Bamberg, K. Schulman, M. MacKenzie, J. Moore, and S. Olchesky, “Effect of adverse storage conditions on performance of glucometer test strips,” *Clinical Laboratory Science*, vol. 18, no. 4, p. 203, 2005.

[69] B. W. Bequette, “Continuous Glucose Monitoring: Real-Time Algorithms for Calibration, Filtering, and Alarms,” *Journal of Diabetes Science and Technology*, vol. 4, no. 2, pp. 404–418, Mar. 2010.

[70] A. E. Panteleon, K. Rebrin, and G. M. Steil, “The Role of the Independent Variable to Glucose Sensor Calibration,” *Diabetes Technology & Therapeutics*, vol. 5, no. 3, pp. 401–410, Jun. 2003.

[71] A. Facchinetti, G. Sparacino, and C. Cobelli, “Enhanced Accuracy of Continuous Glucose Monitoring by Online Extended Kalman Filtering,” *Diabetes Technology & Therapeutics*, vol. 12, no. 5, pp. 353–363, Apr. 2010.

[72] E. J. Knobbe and B. Buckingham, “The Extended Kalman Filter for Continuous Glucose Monitoring,” *Diabetes Technology & Therapeutics*, vol. 7, no. 1, pp. 15–27, Feb. 2005.

[73] D. Boiroux, M. Hagdrup, Z. Mahmoudi, N. K. Poulsen, H. Madsen, and J. B. Jørgensen, “Model identification using continuous glucose monitoring data for type 1 diabetes,” *IFAC-PapersOnLine*, vol. 49, no. 7, pp. 759–764, 2016.

[74] J. Dean and J. Dean, *Big Data, Data Mining, and Machine Learning : Value Creation for Business Leaders and Practitioners*. Somerset, UNITED STATES: Wiley, 2014.

[75] D. E. Holmes, L. C. Jain, and MyiLibrary, *Innovations in machine learning : theory and applications*. Berlin: Berlin : Springer-Verlag, 2006.

[76] Matthew Beecham, “Briefing - AI, machine learning and cars,” *just-auto.com*, 2017.

[77] B. Vaccaro *et al.*, "Application of machine learning methods for prediction of outcomes after cardiac transplantation: insights from the UNOS database," *Circulation*, vol. 134, no. 19, 2016.

[78] E. Ahlqvist *et al.*, "Novel subgroups of adult-onset diabetes and their association with outcomes: a data-driven cluster analysis of six variables," *The Lancet Diabetes & Endocrinology*.

[79] "Implanting beta cell-seeded biomaterial seeded restores insulin production in type 1 diabetes mouse model | Endocrine Society." [Online]. Available: https://www.endocrine.org/news-room/2018/implanting-beta-cell-seeded-biomaterial-seeded-restores-insulin-production-in-type-1-diabetes-mouse. [Accessed: 04-Apr-2018].

[80] "Medtronic passes US FDA approval for closed loop insulin delivery system MiniMed 670G with SmartGuard HCL algorithm for Type 1 Diabetes," *M2 Pharma*, 2016.

[81] "US FDA approves Abbott's FreeStyle Libre Flash Glucose Monitoring System," *PharmaBiz*, 2017.

[82] S. J. Russell *et al.*, "Outpatient Glycemic Control with a Bionic Pancreas in Type 1 Diabetes," *New England Journal of Medicine*, vol. 371, no. 4, pp. 313–325, Jul. 2014.

[83] S. J. Russell *et al.*, "Day and night glycaemic control with a bionic pancreas versus conventional insulin pump therapy in preadolescent children with type 1 diabetes: a randomised crossover trial," *The Lancet Diabetes & Endocrinology*, vol. 4, no. 3, pp. 233–243, Mar. 2016.

[84] F. H. El-Khatib *et al.*, "Home use of a bihormonal bionic pancreas versus insulin pump therapy in adults with type 1 diabetes: a multicentre randomised crossover trial," *The Lancet*, vol. 389, no. 10067, pp. 369–380, Jan. 2017.

[85] R. Rastogi, A. Dehennis, X. O. Chen, D. Mullen, and R. M. Bergenstal, "Continuous Glucose Monitoring for 90 days: How Stable are Time in Range and Glucose Patterns?," p. 1.

[86] A. Sadana and A. Madagula, "A fractal analysis of external diffusion limited first-order kinetics for the binding of antigen by immobilized antibody," *Biosensors and Bioelectronics*, vol. 9, no. 1, pp. 45–55, 1994.

[87] P. De Meyts and G. G. Rousseau, "Receptor concepts. A century of evolution.," *Circulation research*, vol. 46, no. 6 Pt 2, p. I3, 1980.

[88] J. T. La Belle, A. Fairchild, U. K. Demirok, and A. Verma, "Method for fabrication and verification of conjugated nanoparticle-antibody tuning elements

for multiplexed electrochemical biosensors," *Methods*, vol. 61, no. 1, pp. 39–51, 2013.

[89] C. T. Christoffersen *et al.*, "Negative cooperativity in the insulin-like growth factor-I receptor and a chimeric IGF-I/ insulin receptor," *Endocrinology.*, vol. 135, no. 1, pp. 472–475, Jul. 1994.

[90] S. Rousseau-Migneron, A. Nadeau, and G. Tancrède, "Effects of isoproterenol on insulin and glucagon secretion in rats treated chronically with isoproterenol," *Can. J. Physiol. Pharmacol.*, vol. 58, no. 3, pp. 275–280, Mar. 1980.

[91] J. T. Labelle, "A Multi-Marker Approach for Improved Glycemic Management in Diabetes Mellitus," *Journal of Diabetes, Metabolic Disorders & Control*, vol. 4, no. 5, Aug. 2017.

[92] J. T. La Belle, J. Q. Gerlach, S. Svarovsky, and L. Joshi, "Label-free impedimetric detection of glycan− lectin interactions," *Analytical chemistry*, vol. 79, no. 18, pp. 6959–6964, 2007.

[93] C. Lin, L. Ryder, D. Probst, M. Caplan, M. Spano, and J. LaBelle, "Feasibility in the development of a multi-marker detection platform," *Biosensors and Bioelectronics*, vol. 89, pp. 743–749, 2017.

[94] S. Kochowski and K. Nitsch, "Description of the frequency behaviour of metal–SiO2–GaAs structure characteristics by electrical equivalent circuit with constant phase element," *Thin Solid Films*, vol. 415, no. 1–2, pp. 133–137, Aug. 2002.

[95] B. Hirschorn, M. E. Orazem, B. Tribollet, V. Vivier, I. Frateur, and M. Musiani, "Determination of effective capacitance and film thickness from constant-phase-element parameters," *Electrochimica Acta*, vol. 55, no. 21, pp. 6218–6227, Aug. 2010.

[96] C. H. Hsu and F. Mansfeld, "Technical Note:Concerning the Conversion of the Constant Phase Element Parameter Yo into a Capacitance," *Corrosion*, vol. 57, no. 9, pp. 747–748, Sep. 2001.

[97] Z. Chen and A. Sadana, "An analysis of antigen-antibody binding kinetics for biosensor applications utilized as a model system: influence of non-specific binding," *Biophysical chemistry*, vol. 57, no. 2–3, pp. 177–187, 1996.

[98] "Factors affecting the antigen-antibody reaction." [Online]. Available: https://www-ncbi-nlm-nih-gov.ezproxy1.lib.asu.edu/pmc/articles/PMC2581910/. [Accessed: 23-Apr-2018].

[99] A. Sadana and A. M. Beelaram, "Antigen-antibody diffusion-limited binding kinetics of biosensors: a fractal analysis," *Biosensors and Bioelectronics*, vol. 10, no. 3–4, pp. 301–316, 1995.

[100] J. Y. Gerasimov, C. S. Schaefer, W. Yang, R. L. Grout, and R. Y. Lai, "Development of an electrochemical insulin sensor based on the insulin-linked polymorphicregion," *Biosensors and Bioelectronics*, vol. 42, pp. 62–68, 2013.

[101] T. L. Adamson, F. A. Eusebio, C. B. Cook, and J. T. LaBelle, "The promise of electrochemical impedance spectroscopy as novel technology for the management of patients with diabetes mellitus," *Analyst*, vol. 137, no. 18, pp. 4179–4187, 2012.

[102] T. L. Adamson, C. B. Cook, and J. T. LaBelle, "Detection of 1, 5-anhydroglucitol by electrochemical impedance spectroscopy," *Journal of diabetes science and technology*, vol. 8, no. 2, pp. 350–355, 2014.

[103] A. B. Fairchild, K. McAferty, U. K. Demirok, and J. T. La Belle, "A label-free, rapid multimarker protein impedance-based immunosensor," in *Complex Medical Engineering, 2009. CME. ICME International Conference on*, 2009, pp. 1–5.

[104] K. Bhavsar *et al.*, "A cytokine immunosensor for Multiple Sclerosis detection based upon label-free electrochemical impedance spectroscopy using electroplated printed circuit board electrodes," *Biosensors and Bioelectronics*, vol. 25, no. 2, pp. 506–509, 2009.

[105] U. K. Demirok, A. Verma, and J. T. L. Belle, "The Development of a Label-Free Electrochemical Impedance Based Pointof-care Technology for Multimarker Detection," *Journal of Biosensors & Bioelectronics*, vol. 0, no. 0, pp. 1–7, May 2013.

[106] J. T. La Belle, U. K. Demirok, D. R. Patel, and C. B. Cook, "Development of a novel single sensor multiplexed marker assay," *Analyst*, vol. 136, no. 7, pp. 1496–1501, 2011.

[107] A. V. Patil, F. C. Bedatty Fernandes, P. R. Bueno, and J. J. Davis, "Immittance electroanalysis in diagnostics," *Analytical chemistry*, vol. 87, no. 2, pp. 944–950, 2014.

[108] Y. Boonyasit, O. Chailapakul, and W. Laiwattanapaisal, "A multiplexed three-dimensional paper-based electrochemical impedance device for simultaneous label-free affinity sensing of total and glycated haemoglobin: The potential of using a specific single-frequency value for analysis," *Analytica chimica acta*, vol. 936, pp. 1–11, 2016.

[109] A. L. Rinaldi and R. Carballo, "Impedimetric non-enzymatic glucose sensor based on nickel hydroxide thin film onto gold electrode," *Sensors and Actuators B: Chemical*, vol. 228, pp. 43–52, 2016.

[110] G.-H. Hui, P. Ji, S.-S. Mi, and S.-P. Deng, "Electrochemical impedance spectrum frequency optimization of bitter taste cell-based sensors," *Biosensors and Bioelectronics*, vol. 47, pp. 164–170, 2013.

[111] G. R. Kasaliwal, A. Göldel, P. Pötschke, and G. Heinrich, “Influences of polymer matrix melt viscosity and molecular weight on MWCNT agglomerate dispersion,” *Polymer*, vol. 52, no. 4, pp. 1027–1036, 2011.

[112] P. R. Solanki, A. Kaushik, V. V. Agrawal, and B. D. Malhotra, “Nanostructured metal oxide-based biosensors,” *NPG Asia Materials*, vol. 3, no. 1, p. 17, 2011.

[113] Y. Boonyasit, W. Laiwattanapaisal, O. Chailapakul, J. Emnéus, and A. R. Heiskanen, “Boronate-modified interdigitated electrode array for selective impedance-based sensing of glycated hemoglobin,” *Analytical chemistry*, vol. 88, no. 19, pp. 9582–9589, 2016.

[114] B. Pamornpathomkul, A. Wongkajornsilp, W. Laiwattanapaisal, T. Rojanarata, P. Opanasopit, and T. Ngawhirunpat, “A combined approach of hollow microneedles and nanocarriers for skin immunization with plasmid DNA encoding ovalbumin,” *Int J Nanomedicine*, vol. 12, pp. 885–898, 2017.

[115] C. G. Koops, “On the dispersion of resistivity and dielectric constant of some semiconductors at audiofrequencies,” *Physical Review*, vol. 83, no. 1, p. 121, 1951.

[116] K. S. Cole and R. H. Cole, “Dispersion and absorption in dielectrics I. Alternating current characteristics,” *The Journal of chemical physics*, vol. 9, no. 4, pp. 341–351, 1941.

[117] O. Pillai, S. D. Borkute, N. Sivaprasad, and R. Panchagnula, “Transdermal iontophoresis of insulin: II. Physicochemical considerations,” *International journal of pharmaceutics*, vol. 254, no. 2, pp. 271–280, 2003.

[118] G. W. Lu and P. Gao, “Emulsions and microemulsions for topical and transdermal drug delivery,” in *Handbook of Non-Invasive Drug Delivery Systems*, Elsevier, 2010, pp. 59–94.

[119] B. Sudharsan, M. Peeples, and M. Shomali, “Hypoglycemia prediction using machine learning models for patients with type 2 diabetes,” *Journal of diabetes science and technology*, vol. 9, no. 1, pp. 86–90, 2015.

[120] A. B. Olokoba, O. A. Obateru, and L. B. Olokoba, “Type 2 Diabetes Mellitus: A Review of Current Trends,” *Oman Medical Journal*, vol. 27, no. 4, pp. 269–273, Jul. 2012.

[121] E. S. Huang, A. Basu, M. O’Grady, and J. C. Capretta, “Projecting the future diabetes population size and related costs for the US,” *Diabetes care*, vol. 32, no. 12, pp. 2225–2229, 2009.

[122] A. P. Turner, “Biosensors--sense and sensitivity,” *Science*, vol. 290, no. 5495, pp. 1315–1317, 2000.

[123] S. P. Juraschek, M. W. Steffes, and E. Selvin, “Associations of alternative markers of glycemia with hemoglobin A1c and fasting glucose,” *Clinical chemistry*, vol. 58, no. 12, pp. 1648–1655, 2012.

[124] M. L. Larsen, M. Hørder, and E. F. Mogensen, “Effect of long-term monitoring of glycosylated hemoglobin levels in insulin-dependent diabetes mellitus,” *New England Journal of Medicine*, vol. 323, no. 15, pp. 1021–1025, 1990.

[125] R. A. Boer *et al.*, “Predictive value of plasma galectin-3 levels in heart failure with reduced and preserved ejection fraction,” *Annals of medicine*, vol. 43, no. 1, pp. 60–68, 2011.

[126] S. D. Sullivan, L. P. Garrison Jr, H. Rinde, J. Kolberg, and E. J. Moler, “Cost-effectiveness of risk stratification for preventing type 2 diabetes using a multi-marker diabetes risk score,” *Journal of medical economics*, vol. 14, no. 5, pp. 609–616, 2011.

[127] T. J. Wang *et al.*, “Multiple biomarkers and the risk of incident hypertension,” *Hypertension*, vol. 49, no. 3, pp. 432–438, 2007.

[128] T. J. Wang *et al.*, “Multiple biomarkers for the prediction of first major cardiovascular events and death,” *New England Journal of Medicine*, vol. 355, no. 25, pp. 2631–2639, 2006.

[129] E. D. Rosen and B. M. Spiegelman, “Adipocytes as regulators of energy balance and glucose homeostasis,” *Nature*, vol. 444, no. 7121, pp. 847–853, 2006.

[130] D. Rodbard, “Evaluating Quality of Glycemic Control Graphical Displays of Hypo-and Hyperglycemia, Time in Target Range, and Mean Glucose,” *Journal of diabetes science and technology*, vol. 9, no. 1, pp. 56–62, 2015.

[131] E. S. Kilpatrick, P. W. Maylor, and B. G. Keevil, “Biological variation of glycated hemoglobin: implications for diabetes screening and monitoring,” *Diabetes Care*, vol. 21, no. 2, pp. 261–264, 1998.

[132] T. L. Adamson, C. B. Cook, and J. T. LaBelle, “Detection of 1,5-Anhydroglucitol by Electrochemical Impedance Spectroscopy,” *Journal of Diabetes Science and Technology*, vol. 8, no. 2, pp. 350–355, Mar. 2014.

[133] T. L. Adamson, F. A. Eusebio, C. B. Cook, and J. T. LaBelle, “The promise of electrochemical impedance spectroscopy as novel technology for the management of patients with diabetes mellitus,” *Analyst*, vol. 137, no. 18, pp. 4179–4187, 2012.

[134] M. Xu, X. Luo, and J. J. Davis, “The label free picomolar detection of insulin in blood serum,” *Biosensors and Bioelectronics*, vol. 39, no. 1, pp. 21–25, Jan. 2013.

[135] X. Luo, M. Xu, C. Freeman, T. James, and J. J. Davis, "Ultrasensitive label free electrical detection of insulin in neat blood serum," *Analytical chemistry*, vol. 85, no. 8, pp. 4129–4134, 2013.

[136] E. Martínez-Periñán *et al.*, "Insulin sensor based on nanoparticle-decorated multiwalled carbon nanotubes modified electrodes," *Sensors and Actuators B: Chemical*, vol. 222, pp. 331–338, 2016.

[137] C. Lin, L. Ryder, D. Probst, M. Caplan, M. Spano, and J. LaBelle, "Feasibility in the development of a multi-marker detection platform," *Biosensors and Bioelectronics*, 2016.

[138] A. Ulman, "Formation and structure of self-assembled monolayers," *Chemical reviews*, vol. 96, no. 4, pp. 1533–1554, 1996.

[139] Y. Pan *et al.*, "Electrochemical immunosensor detection of urinary lactoferrin in clinical samples for urinary tract infection diagnosis," *Biosensors and Bioelectronics*, vol. 26, no. 2, pp. 649–654, 2010.

[140] Y. Lu *et al.*, "Olfactory biosensor using odorant-binding proteins from honeybee: Ligands of floral odors and pheromones detection by electrochemical impedance," *Sensors and Actuators B: Chemical*, vol. 193, pp. 420–427, Mar. 2014.

[141] E. Barsoukov and J. R. Macdonald, *Impedance spectroscopy: theory, experiment, and applications*. John Wiley & Sons, 2005.

[142] B. Kuznetsov, G. Shumakovich, O. Koroleva, and A. Yaropolov, "On applicability of laccase as label in the mediated and mediatorless electroimmunoassay: effect of distance on the direct electron transfer between laccase and electrode," *Biosensors and Bioelectronics*, vol. 16, no. 1, pp. 73–84, 2001.

[143] A. Malkoc, E. Sanchez, M. R. Caplan, and J. T. La Belle, "Electrochemical-Nucleic Acid Detection with Enhanced Specificity and Sensitivity," *Journal of Biosensors & Bioelectronics*, vol. 6, no. 2, p. 1, 2015.

[144] G. Freckmann, C. Schmid, A. Baumstark, S. Pleus, M. Link, and C. Haug, "System accuracy evaluation of 43 blood glucose monitoring systems for self-monitoring of blood glucose according to DIN EN ISO 15197," *Journal of diabetes science and technology*, vol. 6, no. 5, pp. 1060–1075, 2012.

[145] G. Hajisalem, Q. Min, R. Gelfand, and R. Gordon, "Effect of surface roughness on self-assembled monolayer plasmonic ruler in nonlocal regime," *Optics express*, vol. 22, no. 8, pp. 9604–9610, 2014.

[146] Y. Lu *et al.*, "Impedance spectroscopy analysis of human odorant binding proteins immobilized on nanopore arrays for biochemical detection," *Biosensors and Bioelectronics*, vol. 79, pp. 251–257, 2016.

[147] E. Boubour and R. B. Lennox, “Insulating properties of self-assembled monolayers monitored by impedance spectroscopy,” *Langmuir*, vol. 16, no. 9, pp. 4222–4228, 2000.

APPENDIX A

RELEVANT PUBLICATION

Enhancing Glycemic Control via Detection of Insulin using Electrochemical Impedance Spectroscopy

Aldin Malkoc, MS[a], David Probst, MS[a], Chi Lin, MS[a], Mukund Khanwalker, BSE[a], Connor Beck, BSE[a], Curtiss B. Cook M.D.[b], Jeffrey T. La Belle PhD[a,b].

Author Affiliation: [a]School of Biological and Health Systems Engineering, Arizona State University, 550 E. Orange St., Tempe, AZ 85287, USA
[b]School of Medicine, Mayo Clinic Arizona,13400 E. Shea Blvd., Scottsdale, AZ 85259, USA

Aldin Malkoc Arizona State University 550 E. Orange St., Tempe, AZ 85287, USA 602 687 3739 Aldin.malkoc@gmail.com	David Probst Arizona State University 550 E. Orange St., Tempe, AZ 85287, USA 480 399 1273 david.probst@asu.edu	Mukund Khanwalker Arizona State University 550 E. Orange St., Tempe, AZ 85287, USA 480 326 0526 mukund.khanwalker@asu.edu	Connor Beck Arizona State University 550 E. Orange St., Tempe, AZ 85287, USA 208 654 8252 connor.beck@asu.edu
Chi Lin Arizona State University 550 E. Orange St., Tempe, AZ 85287, USA 480 392 8004 chi.lin@asu.edu	Curtiss B. Cook Arizona State University 550 E. Orange St., Tempe, AZ 85287, USA 480 727 9061 curtiss@mayo.edu	Jeffrey T. La Belle Arizona State University 550 E. Orange St. Tempe, AZ 85287, USA 480 727 9061 Jeffrey.labelle@asu.edu	

Abbreviations: DM: Diabetes Mellitus; EDC: 1-Ethyl-3-(3-Dimethylaminopropyl) Carbodiimide; EIS: Electrochemical Impedance Spectroscopy; GDE: Gold Disk Electrode; LLD: Lower Limit of Detection; MHDA: Mercaptohexadecanoic acid; NHS: N-hydroxysuccinimide; OBF: Optimal Binding Frequency; PBS: Phosphate Buffer Saline; POC: Point-of-Care; QC: Quality Control; RSD: Relative Standard Deviation; RSQ: R-square Values; SAM: Self-Assembling Monolayer; SOTA: State of the Art; SPSs: Screen Printed Electrodes.

Keyword: Diabetes Mellitus; Electrochemical Impedance Spectroscopy; Imaginary Impedance; Insulin; Label Free; Point-of-Care;

Corresponding Author: Jeffrey T. La Belle Arizona State University, 550 E. Orange St., Tempe, AZ 85287, USA

Funding Source: The work was funded by Mayo Hospital grant ARI-209490

Conflict-of-Interest Disclosure: None

Acknowledgments: We appreciate the help from the Mayo Clinic, Fulton School of Engineering, and the School of Biological Health and System Engineering.

Figures and Tables Count: 6 figures

Abstract

Background: Currently, glycemic management for individuals with diabetes mellitus involves monitoring glucose only, which is insufficient as glucose metabolism involves other biomarkers such as insulin. Monitoring additional biomarkers alongside glucose has been proposed to improve glycemic control. In this work, the development of a rapid and label-free insulin biosensor with high sensitivity and accuracy is presented. The insulin sensor prototype also serves as a prior study for a multi-marker sensing platform technology that can further improve glycemic control in the future.

Methods: Electrochemical impedance spectroscopy was used to identify an optimal frequency specific to insulin detection on a gold disk electrode with insulin antibody immobilized, which was accomplished by conjugating the primary amines of insulin antibody to the carboxylic bond of the self-assembling monolayer on the gold surface. After blocking with ethanolamine, the insulin physiological concentration gradient was tested. The imaginary impedance was correlated to insulin concentration and the results were compared with standard equivalent circuit analysis and correlation of charge transfer resistance to target concentration.

Results: The optimal frequency of insulin is 810.5 Hz, which is characterized by having the highest sensitivity and sufficient specificity. The lower limit of detection was 2.26 ρM which is comparable to a standard and better than traditional approaches.

Conclusion: An insulin biosensor prototype capable of detecting insulin in physiological range without complex data normalization was developed. This prototype will be the ground works of a multi-marker platform sensor technology for future all-in-one glycemic management sensors.

Introduction

DM encompasses a series of chronic metabolic diseases characterized by inadequate glucose metabolism[119]. It is quickly becoming a worldwide epidemic, involving nearly 30 million people in the United States, and costing nearly 250 billion dollars[120]. According to the American Diabetes Association, by the year 2034 the number of diagnosed and undiagnosed people with diabetes will increase from 23.7 million to 44.1 million[121]. With such an increase in prevalence, there has also been a large need for next generation technology to help manage the disease with better portability and increased sensitivity[122]. Currently, diabetes management involves monitoring glucose levels daily, either discretely or continuously, and glycated hemoglobin (HbA1c) levels periodically[123], [124]. Overall, detection and monitoring of glucose levels is achieved through detection of a single marker: glucose. Recently, there have been strides to develop multi-marker assays due to many studies showing monitoring of multiple biomarkers associated with a complex disease can enhance the accuracy of disease diagnosis, prognosis, management, and treatment[125]–[128]. Figure 1 shows key biomarkers involved in glucose management[123] and measuring of these biomarkers can give a better understanding of a patient's state of health. Additionally, enhanced biomarker detection would extend to the development of multi-marker simultaneous detection on a single POC.

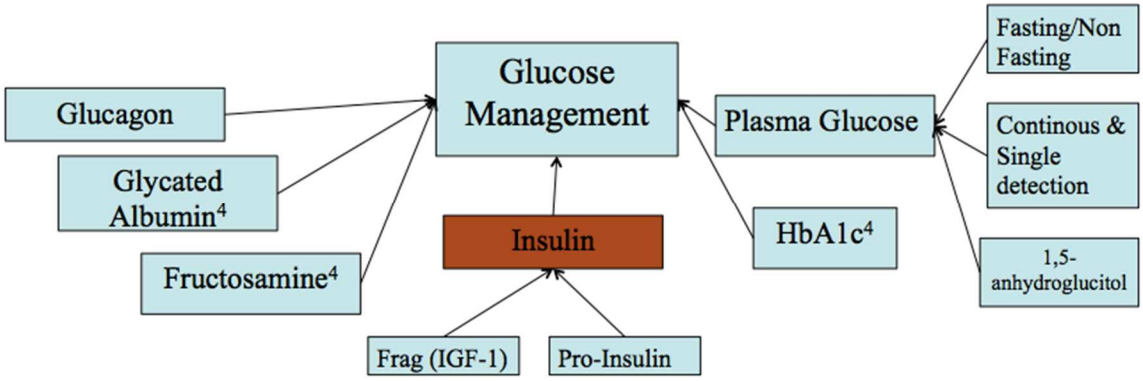

Figure 1: Representation of selective markers that influence glucose management

Among the many biomarkers in Figure 1, insulin is a biomarker that directly affects glucose levels in achieving glucose homeostasis[129]–[131]. The current SOTA for insulin detection are enzyme-linked immunosorbent assay (ELISA) and High Performance Liquid Chromatography (HPLC). While these techniques are specific and sensitive, they require specialized laboratory technicians and time consuming procedures[132], [133]. There is a need for a simple, label free, and rapid insulin sensor suitable for a point-of-care setting in addition to a glucose sensor. In this paper we report the groundwork of a rapid and label-free insulin sensor using EIS.

The momentum on developing electrochemical insulin sensors has been rising in the past few years[100], [134]–[136]. Our group recently showed that, using the imaginary impedance of EIS, a biomarker will have an optimal binding frequency (OBF) at which the change in imaginary impedance best correlates to the change in target concentrations[137]. Furthermore, it would also be possible to measure two biomarkers, for example insulin and glucose, simultaneously by simply monitoring their impedance

response at their respective OBFs, as suggested by our recent work in detecting low and high density lipoproteins simultaneously on a single sensor[137]. We have already characterized glucose previously using EIS and have shown its feasibility in glucose detection[133]. In addition to developing an insulin sensor prototype, this work aims to lay the ground work for a dual marker sensor capable of detecting glucose and insulin simultaneously as suggested previously[137], which would improve glycemic control via controlling glucose and insulin levels concurrently. Once the initial response of insulin is characterized the dual-marker sensor prototype can be developed. Additional biomarkers can be later explored to eventually build a multi-marker sensing platform monitoring all the major biomarkers of DM, providing the most accurate information for medical intervention and glycemic control.

Material and Methods

Reagents and Chemicals

All chemical reagents were purchased from Sigma (St Louis, MO, USA) unless stated otherwise. The 10 mM phosphate buffer saline (PBS) tablets were purchased from Calbiochem (Gibbstown, NJ, USA), potassium hexacyanoferrate (III) from EMD Chemicals (Billerica, MA, USA), and sulfo-derivative of N-hydroxysuccinimide sodium salt (NHS) from Toronto Research Chemicals (Toronto, Ontario, Canada). The redox probe reagent used was 100 mM potassium ferricyanide dissolved in pH 7.4 PBS.

Sensor Fabrication and Testing

The sensor consists of 3 electrodes: working gold disk electrodes (GDEs), reference silver/silver chloride electrodes, and counter platinum electrodes acquired from CH Instruments (Austin, TX, USA). All EIS measurements were performed at room temperature using a CHI660C Electrochemical Analyzer from CH Instrument at the electrode's formal potential from 1 Hz to 100 kHz. A Buehler felt pad with 0.05 μg grit aluminum oxide particles was used to polish the GDEs with 10 figure-eight motions, followed by a 20-minute sonication in deionized water. After electrode polishing, cyclic voltammetry (CV) from -1.0 V to 1.0 V was used to obtain the formal potential and bare electrode EIS was performed to evaluate sensor cleanliness.

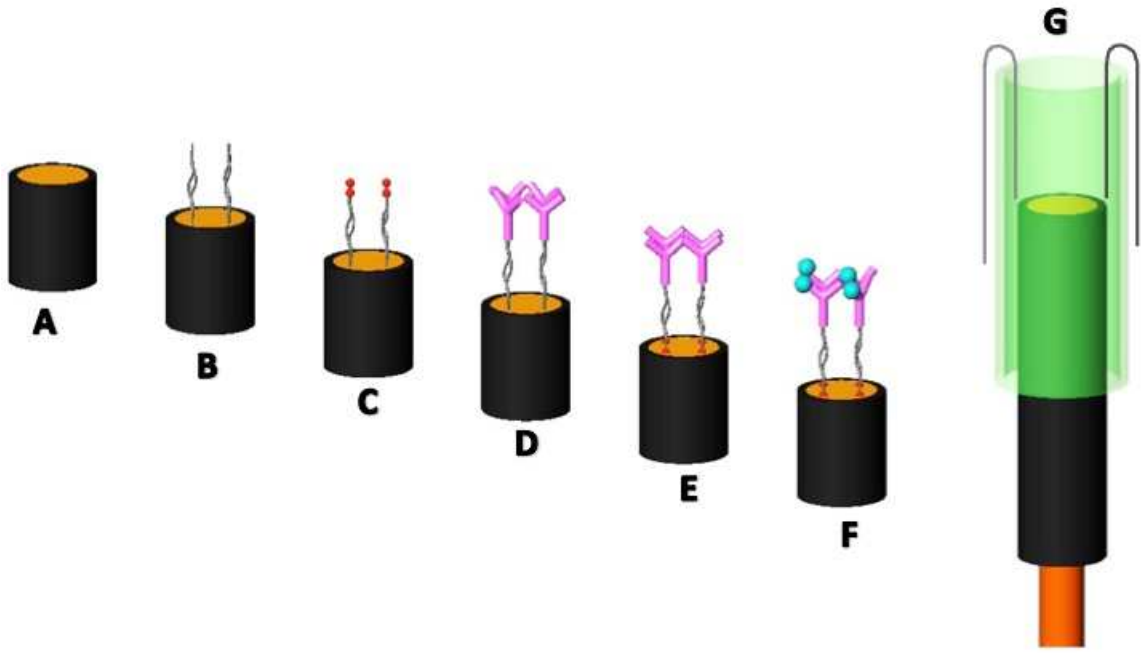

Figure 2 (Scheme): This illustration shows sensor fabrication process and detection mechanism. A: Bare GDE. B: 1 mM 16-MHDA self-assembled linker. C: EDC/NHS coupling. D: immobilization of 156 μM insulin antibody. E: 1% ethanolamine blocking. F: Binding of insulin antigen to antibody. G: Electrochemical cell consists of a 1000 μL pipet tip with counter and reference electrodes.

Once the sensors were cleaned, the SAM was created by incubating 1 mM of 16-mercaptohexadecanoic acid (MHDA) for one hour at room temperature. The sensors were then rinsed and stored dry overnight to ensure proper deposition of SAM, as SAMs takes hours to reach their final thickness and contact angles[138], [139]. The carboxylate groups of the 16-MHDA were activated by incubating the sensor in 10 mM 1-ethyl-3-(3-

dimethylaminopropyl) carbodiimide (EDC) and 80 mM sulfo-NHS for one hour at room temperature. After rinsing with DI, 100 µL of 156 μM of insulin antibody prepared in pH 7.4 PBS was incubated onto the electrode surface for one hour. After rinsing with PBS the sensors were blocked with 1% ethanolamine for 30 minutes to block any remaining active sites, completing the sensor fabrication process. The schematic of sensor preparation can be found in Figure 2. The finished sensors were stored at 277.15 K until testing. All sensors were brought to room temperature before running each test. Insulin antigen gradients were prepared through serial dilution with PBS. Each sample contained 200 mM potassium ferricyanide and equal volume of insulin antigen to form 100 μL total solution volume. Final insulin samples were made according to the physiological concentration range from 0 ρM to 1500 ρM to establish a calibration curve.

Quality Control

Electrodes were prepared in batches of eighteen and all electrodes were analyzed using EIS. After measuring the post-MHDA impedance, the quality control (QC) was executed by selecting only the electrodes with similar peak frequencies and impedance magnitudes that are within 6% to 10% relative standard deviation (%RSD). Only the QC passing sensors would then proceed with immobilization.

Determination of OBF and Circuit Modeling

Once EIS was performed, the imaginary impedance values were correlated to target concentrations to calculate slope and R-square values (RSQ) across the frequency sweep.

The OBF is the frequency at which the slope peaks with RSQ values above 0.85. All circuit modeling was performed using ZsimpWin software.

Results

Using the methods described above, the impedance responses from 7 electrodes were used to determine the OBF of insulin, which was found to be 810.5 Hz (Figure 3). This relationship was evident in all 7 electrodes as the peak frequency shifts consistently comparing to the post-MHDA results (Figure 3a).

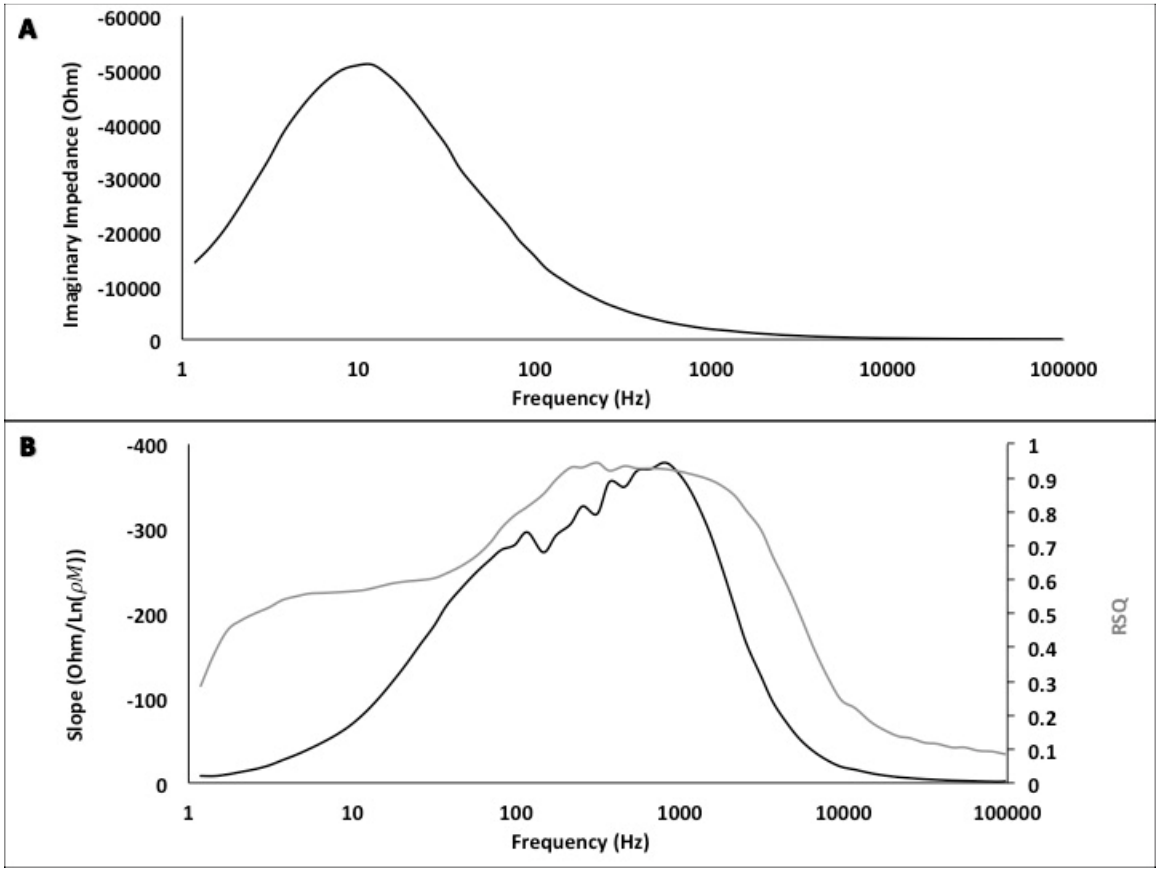

Figure 3: A) This figure is an example of the QC mentioned above, and shows the average peak location, and magnitude of the desired electrodes within the test data. B) This figure shows the logarithmic fit (slope) and RSQ values by fitting the imaginary

impedance against target insulin concentrations across the frequency sweep. 810.5 Hz was found to be the OBF at which both slope and RSQ peaked.

Figure 4 shows the relationship between the imaginary impedance and the target insulin concentration range (0 ρM to 1500 ρM) at the OBF of 810.5 Hz. The target insulin range is the physiological insulin range[140]. The correlations between the impedance and concentrations were 0.926 and the logarithmic slope was -378.1ln(x) with x being the concentration of insulin and the intercept being -5001.1. The slope is represented as negative due to the nature of imaginary impedance values however; the graph represents correlation between increasing concentration and impedance. The %RSDs for this physiological concentration range from low to high concentrations were 11%, 5%, 26%, 19%, 14%, 5%, 5%, 25%, and 16%. The lower limit of detection was calculated to be 2.64 ρM.

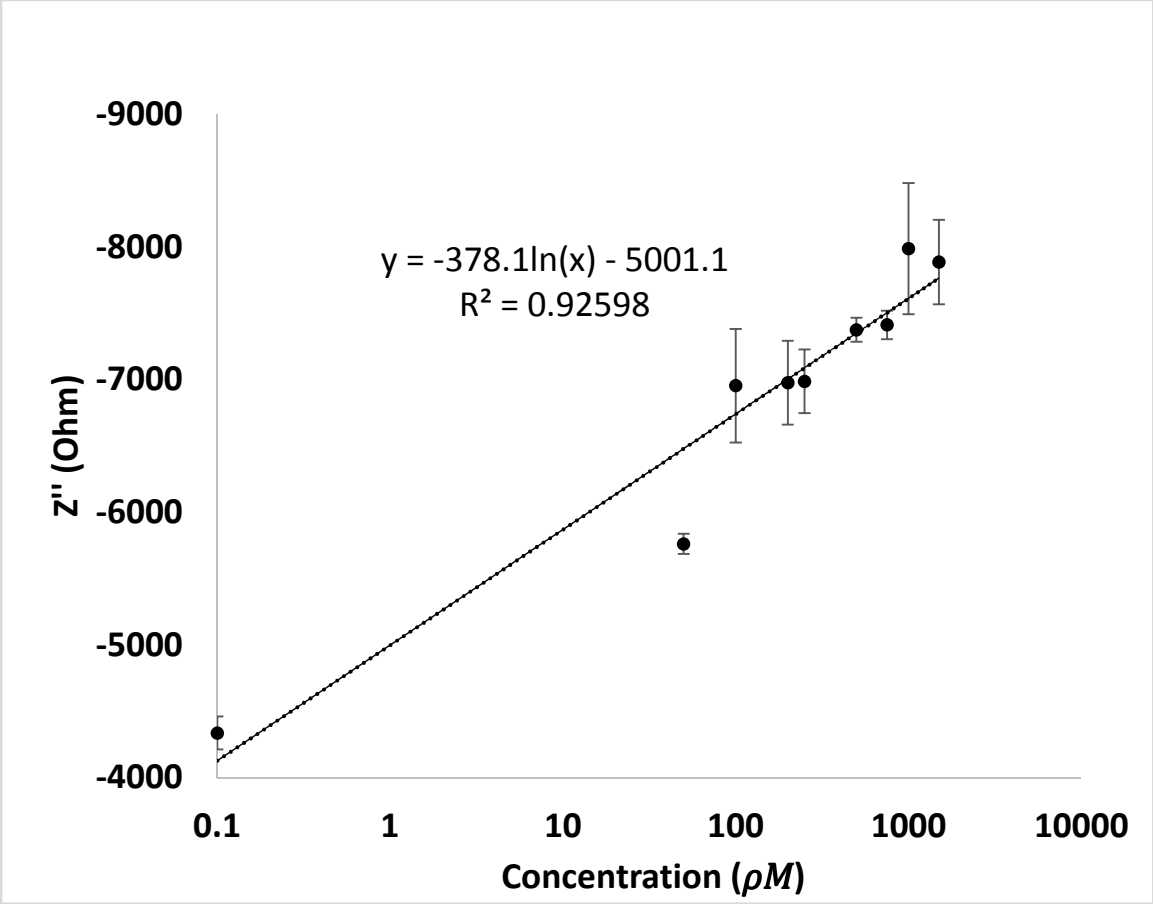

Figure 4: This is a representation of a calibration curve of 0, 50, 100, 200, 250, 500, 750,1000, 1500 ρM based off imaginary impedance readings of insulin detected with N = 7 repetitions at each concentration. Error bars were calculated from the standard deviations.

Using ZsimpWin, the ideal circuit model that best describes the electrochemical system of insulin sensor can be obtained (Figure 5). The solution resistance and the electron transfer resistance were both modeled as resistors and were labeled as R_{sol} and R_{et}, respectively. The pseudo-capacitor is modeled as Q and represents the piece of the system that can be correlated to the molecular recognition element being used[137].

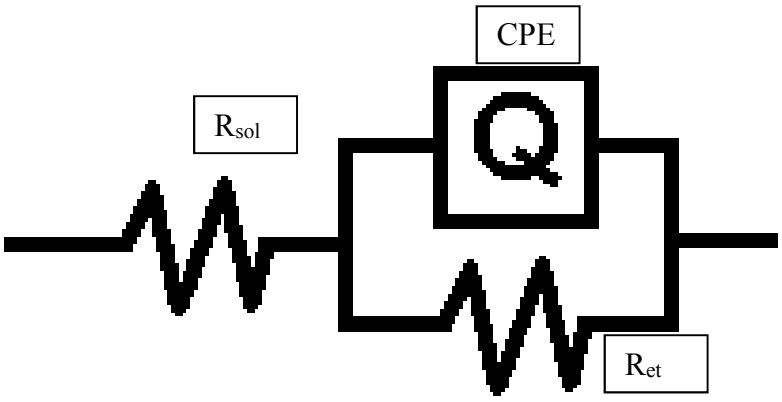

Figure 5: The image above is the circuit used to model the electrochemical cell. R_{sol} is the resistance due to solution, R_{et} is the electron transfer resistance. Q is used to represent the constant phase element (CPE) or the imperfect capacitor of the system.

Figure 6 shows the correlation between charge transfer resistance and target insulin concentrations derived from equivalent circuit modeling, a standard method of analyzing EIS data[141].

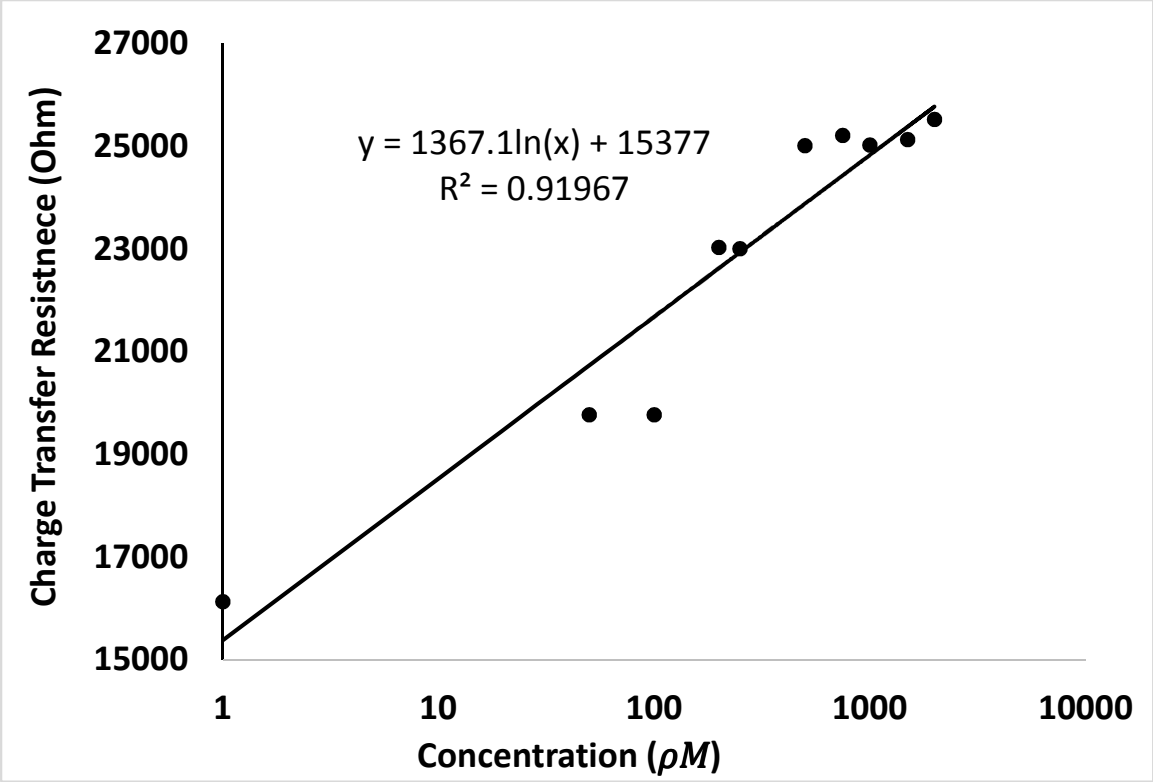

Figure 6: Calibration curve relating the calculated charge transfer resistance against the change in concentration of insulin in ρM.

Discussion

Electrochemical Impedance Results

Comparing the results between Figure 3a and 3b, it was evident that the shift in peak frequency is due to the binding of insulin antibody. The shifts are reproducible as the QC was executed rigorously. Since the slope peaks at 810.5 Hz with RSQ value of 0.93, 810.5 Hz is determined to be the OBF of insulin. However, it is important to note that there is often a trade-off between the sensitivity (slope) and specificity (RSQ) when considering the optimal frequency of EIS[133]. Figure 4 shows the calibration curve for purified insulin at 810.5 Hz. For insulin, a logarithmic fit with slope of -378.1 Ohm/Ln(ρM) and RSQ of 0.93 was found to correlate imaginary impedance with concentration of insulin. The purpose for running a calibration curve experiment is because ideally, a hand held device could be programmed with these equations and upon running EIS on an unknown sample, the calibration curve would convert an imaginary impedance reading into an insulin concentration.

The lower limit of detection (LLD) and dynamic range are important parameters in determining the efficiency of the system. The LLD and dynamic range were calculated based off the standard deviation and slope of the system. The LLD was found to be 2.64 ρM and dynamic range from 50 pM to 1500 pM, which meets clinical needs. From a clinical standard detection of insulin, ELISA can accurately detect labeled insulin at 1.39 ρM [142]. This is slightly lower then what we have demonstrated with this sensor prototype, but with optimization of the electrode design, the LLD may be lowered to that of ELISA. Even more so, techniques such as ELISA or high-performance liquid

chromatography have labeling steps and many associated techniques that can be performed only in laboratories. EIS on the other hand, is a label free technique, and the sensor prototype can be translated into screen printed sensors, allowing the possibility of POC with portable device and disposable test strips similar to the setup of self-monitoring of blood glucose[132], [143].

The Food and Drug Administration requires all glucose meters to be within 20% variance from standards[144]. Currently, the replicated results show that across all sample concentrations the %RSDs ranges from 5% to 26%, suggesting there are still room for improvements. Although batch analysis has helped eliminate some of the variance between GDEs, polishing and reusing GDEs is a significant source of variance as surface roughness of gold can affect SAM formation[145], affecting the capacitance of imperfect parallel plate capacitor (IPPC) explained in later section. Transition to screen printed sensors will reduce the variance of surface roughness under consistent manufacturing procedures and rigorous QC.

We have shown that the EIS method of using imaginary impedance can very well detect insulin in the physiological range. Future studies will look into replicating the trials with much smaller concentration interval sizes such as 1 *p*M, which is equivalent to a gold standard ELISA to distinguish between even the smallest changes in concentration. Interference and clinical samples will also be tested to evaluate robustness and optimize further toward a POC device. This will lay a solid foundation for the multi-marker platform sensor to truly enhance a person's glycemic control. Lastly, unlike other

publications on insulin detection there was no modification to the insulin solution via pH[134], [135].

Circuit Analysis

Generally, EIS is analyzed with equivalent circuit modeling. Typically, the best-fit circuit for a semi-circle looking Nyquist plot is the Randles circuit, which models the electrochemical interactions as a resistance-capacitor circuit in parallel. The electron transfer resistance can be used to derive a calibration curve linking back to input concentration[88], [142]. However, recently some researchers have demonstrated the use of a modified Randles circuit that implements a constant phase element (CPE) to model the capacitance[137], [140], [146]. CPE is commonly referred to as either a leaky or imperfect parallel plate capacitor (IPPC). The bottom plate is the surface of electrode and the top plate is the top of the SAM with MREs immobilized owing to SAM's insulating property[147]. The MREs different shape, orientation and size alter the smoothness of SAM in various ways, constituting the IPPC. As binding occurs, the target-MRE complex further alters the capacitance of the IPPC, affecting the electron transferring properties and impedance signals, which is evident in Figure 6. This model gives a better description of the actual system when compared to the ideal Randles. Since imaginary impedance correlates to capacitance[141], we used imaginary impedance to correlate target concentration to reflect the impedance signal generated from changes in CPE, which we believe to have less noise than using the complex impedance approach and omits the trouble of circuit modeling. Owing to this nature, it's no surprise that the LLD in imaginary impedance (2.64 ρM) is lower than that of the complex impedance approach

(14.46 ρM).

Conclusion

An insulin biosensor prototype that has the potential to serve as a POC device alongside with glucose has been developed. Detection of insulin and other markers affecting individuals with diabetes will greatly enhance the ability of individuals with diabetes to better control their own blood glucose levels. With a reproducible LLD of 2.26 ρM the study suggests that imaginary impedance based techniques are not only sensitive enough to detect physiological concentrations in purified solution of small proteins such as insulin but can also compete with current SOTA as well.

Future work includes transitioning to a disposable strip that is capable of insulin detection in clinical samples. Currently, we are starting to make screen printed electrodes (SPEs) using a MPM Accuflex Speedline screen printer in house. Depending on the dimension of the sensor, machine overhead and the amount of sensors fabricated, the current cost of a sensor can be as low as 1$ per sensor with order size of 45,000 sensors. We hope to translate the insulin sensor prototype onto the SPEs manufactured in house to enhance quality control and obtain a more practical insulin sensor prototype that can be translated to industrial mass manufacturing. Additionally, once the insulin sensor has been truly optimized, the next step would be the design of dual-marker detection sensor using the imaginary impedance of EIS to detect glucose and insulin simultaneously at their respective OBFs. This would be ground breaking and would potentially provide next generation glycemic control to many individuals with diabetes.

Funding Source: The work was funded by Mayo Hospital grant ARI-209490

Conflict-of-Interest Disclosure: None

Acknowledgments: We appreciate the help from the Mayo Clinic, Fulton School of Engineering, and the School of Biological Health and System Engineering.